

UNIVERSIDADE FEDERAL DE MINAS GERAIS
ESCOLA DE ENGENHARIA
PROGRAMA DE PÓS-GRADUAÇÃO EM ENGENHARIA DE ESTRUTURAS

Mariana Pimenta Alves

**Effect of In-Plane Fiber Waviness in Unidirectional CFRP
Composites**

2017

Mariana Pimenta Alves

**Effect of In-plane Fiber Waviness in Unidirectional CFRP
Composites**

Dissertation submitted to the Post Graduate Program in Structural Engineering of Universidade Federal de Minas Gerais, in partial fulfillment of the requirements for the degree of “Master in Structural Engineering”.

Advisor: Prof. Dr. Carlos Alberto Cimini Jr

Belo Horizonte

2017

A474e	<p>Alves, Mariana Pimenta. Effect of in-plane fiber waviness in unidirectional CFRP composites [manuscrito] / Mariana Pimenta Alves. – 2017. xv, 51 f., enc.: il.</p> <p>Orientador: Carlos Alberto Cimini Jr.</p> <p>Dissertação (mestrado) - Universidade Federal de Minas Gerais, Escola de Engenharia.</p> <p>Anexos: f. 44-51.</p> <p>Bibliografia: f. 41-43.</p> <p>1. Engenharia de estruturas - Teses. 2. Compósitos poliméricos - Teses. 3. Fibras de carbono - Teses. 4. Método dos elementos finitos - Teses. I. Cimini Júnior, Carlos Alberto. II. Universidade Federal de Minas Gerais. Escola de Engenharia. III. Título.</p> <p>CDU: 624(043)</p>
-------	--

UNIVERSIDADE FEDERAL DE MINAS GERAIS
ESCOLA DE ENGENHARIA
PROGRAMA DE PÓS GRADUAÇÃO EM ENGENHARIA DE ESTRUTURAS

Effect of In-plane Fiber Waviness in Unidirectional CFRP Composites

Mariana Pimenta Alves

Dissertation submitted to the Post Graduate Program in Structural Engineering of Universidade Federal de Minas Gerais, in partial fulfillment of the requirements for the degree of “Master in Structural Engineering”.

Dissertation Committee:

Prof. Carlos Alberto Cimini Jr
DEES-UFMG – (Advisor)

Prof. Tulio Hallak Panzera
PPMEC-UFSJ

Prof. Estevam Barbosa de Las Casas
DEES-UFMG

Belo Horizonte, 27 de setembro de 2017

ACKNOWLEDGEMENTS

First of all, I would like to express my sincere gratitude to Professor Dr. Carlos Cimini Jr for the support and comprehension throughout this journey, going far beyond technical assistance. Thank you for never forgetting the human side of our job.

Thank you to Professor Dr. Sung Kyu Ha for the scientific contributions and guidance that made this work richer.

I am grateful to Professor Estevam Las Casas for kindly welcoming me in MECBIO lab and team.

I thank all my fellow students with whom I have shared moments of pure joy and stress, sometimes all together. Researching is a collective work and without your support and inspiration I wouldn't have reached this far.

Thank you to the professors and employees of PROPEEs for the direct contribution in my intellectual and personal growth.

I am grateful to EMBRAER S.A. and CAPES for their financial support.

I would like to express my appreciation to my loving family who cheers me on. And last but not least, thanks to my dear husband Rafael Brasil for the endless affection and support. You are my daily inspiration to become a better person.

RESUMO

Este trabalho consiste em uma investigação sobre os efeitos das ondulações das fibras nas principais propriedades estruturais de compósitos reforçados com fibras de carbono. As ondulações das fibras são um tipo de defeito de fabricação comumente encontrado em componentes de material composto. Modelagem em elementos finitos utilizando a plataforma comercial Abaqus® foi empregada pra simular lâminas unidirecionais contendo ondulações graduais no plano da peça com forma de ondas senoidais. O máximo ângulo de desalinhamento foi tomado como único parâmetro de influência a ser analisado nas simulações. Foi realizada a geração automática dos modelos por meio do uso de scripts em linguagem paramétrica em Python. Os compósitos foram então sujeitos a condições de carregamento e de contorno no plano, com as análises sendo divididas em cargas uniaxiais normais longitudinais/transversais e biaxiais normais. O objetivo era estabelecer uma metodologia computacional eficiente para dar suporte a decisões de controle de qualidade. Os resultados provaram que a curvatura da fibra afeta a distribuição local dos esforços, o que resulta em concentração/relaxamento das tensões originais e induz a ocorrência de tensões locais de natureza diferente das encontradas em placas sem defeito. A influência demonstrada nas propriedades efetivas de rigidez mostrou-se menos significativa que a obtida nos valores de resistência. O início da falha foi determinado por meio da aplicação do critério de falha de Hashin, que faz a distinção entre falhas ocorridas na matriz e na fibra do compósito. Foi observada uma redução de resistência à medida que se aumenta o ângulo de desalinhamento das fibras, favorecendo um modo de falha dominado pelo comportamento da matriz. Carregamentos longitudinais apresentaram maior redução na resistência comparativamente a cargas transversais. Em relação aos carregamentos biaxiais, o caso de carga tração longitudinal + compressão transversal foi o mais severamente afetado em termos de falha; o caso compressão longitudinal + tração transversal mostrou-se como o menos afetado.

Palavras chave: Compósitos reforçados por fibras, Defeitos, Ondulações de Fibras, Análise de Elementos Finitos

ABSTRACT

This work investigates the effects of fiber waviness in key structural properties of carbon fiber reinforced plastic (CFRP) composites. Fiber waviness is a type of manufacturing defect commonly found in composite material parts. Finite element modeling using the commercial platform Abaqus® was performed to simulate unidirectional laminae containing in-plane graded undulations in the shape of sinusoidal waves. The peak misalignment angle was taken as sole influence parameter. Automated model generation was performed through the use of parametric Python scripting. Composites were subjected to in-plane loading and boundary conditions, with analyses being divided into uniaxial normal longitudinal/transverse and biaxial normal loads. The goal was to provide a computationally efficient analysis framework to support decisions in quality control. Results proved that fiber curvature affects local stresses distribution, leading to stress concentration/relaxation and inducing the occurrence of local stresses other than the original ones found in laminae with no defect. The influence on effective elastic modulus was less significant than on strength values. Initial failure was predicted by Hashin failure criterion, which distinguishes between fiber and matrix failure. A strength knockdown effect was observed as misalignment angle increased, favouring a matrix dominated failure mode. Longitudinal load cases presented a higher strength reduction than observed on transverse loading. Regarding biaxial loads, the case of longitudinal tension + transverse compression was the most severely affected in terms of failure; the case of longitudinal compression + transverse tension was the least susceptible one.

Key words: Fiber reinforced composites, Defect, Fiber Waviness, Finite Element Analysis.

TABLE OF CONTENTS

ACKNOWLEDGEMENTS	iii
RESUMO	iv
ABSTRACT	v
LIST OF FIGURES	viii
LIST OF TABLES	xii
LIST OF NOMENCLATURE	xiii
LIST OF ACRONYMS	xv
Introduction	1
1.1 Background.....	1
1.2 Objectives.....	2
1.3 Justification	2
1.4 Methodology.....	2
Literature review.....	4
2.1 Variability and defects in composites	4
2.2 Waviness	6
2.2.1 General aspects	6
2.2.2 Manufacturing aspects.....	10
2.2.3 Waviness forming mechanism	10
2.3 Bibliographic Review	11
2.3.1 The contribution of Hsiao and Daniel	11
2.3.2 The contribution of Cimini Jr	12
2.3.3 The contribution of Garnich and Karami.....	13
2.3.4 The contribution of Altmann <i>et. al</i>	15
2.3.5 The contribution of Lemanski and Sutcliffe	15
Numerical approach.....	18
3.1 Waviness geometry characterization.....	18
3.2 Finite element modeling approach	20
3.3 Failure Criteria.....	23
Results and discussion	25
4.1 Uniaxial normal longitudinal loaded laminae	25
4.2 Uniaxial normal transverse loaded laminae.....	29
4.3 Biaxial normal loaded laminae	32

Conclusions and recommendations	39
5.1 Conclusions	39
5.2 Recommendations for future work.....	40
References	41
APPENDICES	44
Simulation detailed results – Stress distribution	44
Uniaxial normal longitudinal loaded laminae	44
Very severe defects ($\bar{\phi} = 40^\circ$).....	44
Moderate defects ($\bar{\phi} = 5^\circ$)	45
Uniaxial normal transverse loaded laminae.....	47
Very severe defects ($\bar{\phi} = 40^\circ$).....	47
Moderate defects ($\bar{\phi} = 5^\circ$)	48
Simulation detailed results – Critical HFC index examination	50
Very severe defects ($\bar{\phi} = 40^\circ$).....	50
Severe defects ($\bar{\phi} = 20^\circ$).....	50
Moderate defects ($\bar{\phi} = 5^\circ$)	51

LIST OF FIGURES

Figure 1 – Major carbon fiber reinforced plastic (CFRP) and thermoplastics application in AIRBUS A380 (https://composite.wordpress.com/).....	1
Figure 2 - Typical deviations from the designed part geometry (POTTER, 2009).....	5
Figure 3 – Cause and effect diagram of variability and defects in composite materials.	5
Figure 4 – (a) In and out-of-plane waviness configuration (SUTCLIFFE <i>et al.</i> , 2012); (b) Out-of-plane waviness from cut micrograph (HALLANDER <i>et al.</i> , 2013); (c) In-plane waviness from surface micrograph (FARNAND, 2016)	6
Figure 5 – (a) In-plane waviness in a fabric specimen (POTTER, 2009); (b) In-plane waviness in unidirectional material processed by RTM (POTTER, 2009); (c) In-plane waviness in a single-ply laminate of Carbon/Epoxy processed by RTM (MANDELL <i>et al.</i> , 2012).....	7
Figure 6 - 3D surface map of distributed resin pockets measured by near infrared hyperspectral imaging method (ELHAJJAR <i>et al.</i> , 2016).....	8
Figure 7 – Schematic of the fabrication method to create in-plane waviness. The movable cylinder can translate in the 2-direction, while the fixed cylinders can't move (CHAKRAPANI <i>et al.</i> , 2014)	9
Figure 8 – Method used to fabricate a specimen with in-plane FW and photograph of the induced defect (adapted from MIZUKAMI <i>et al.</i> , 2016).....	9
Figure 9 - Representative volume and coordinates for a unidirectional composite with uniform waviness (HISAO and DANIEL, 1996)	12
Figure 10 – Springs-in-series approach (CIMINI JR, 1997).....	13
Figure 11 - A comparison between the three-dimensional wavy unit cell modelling and the straight unit cell with wavy material orientation (KARAMI and GARNICH, 2005)	14
Figure 12 – Compressive strength of uniform and graded ply waviness (ALTMANN <i>et al.</i> 2015).....	15
Figure 13 – Model of random waviness taken from RTM components: (a) initial misalignment angle; (b) von Mises stress distribution during elastic loading, (c) von Mises stress distribution after peak loading (LEMANSKI and SUTCLIFFE, 2012).....	16
Figure 14 - Wave profile and its main geometric features.	18
Figure 15 – Lamina parametric geometry.	19
Figure 16 – Resulting geometries for the different severity of defects investigated.....	20

Figure 17 – FE element mesh (Lamina with $\bar{\phi} = 20^\circ$).	21
Figure 18 - Material orientation of a portion of the FE mesh. Local 1-axis points to fiber direction in agreement with wavy profile.	21
Figure 19 – Load and boundary conditions groups (for compressive cases): (a) lamina under uniaxial normal longitudinal load; (b) lamina under uniaxial normal transverse load; (c) lamina under biaxial normal loads.	22
Figure 20 – Simulated load cases and corresponding text description and ID.	23
Figure 21 – Failure modes in unidirectional fiber composites (CARLSSON <i>et al.</i> , 2013; HASHIN, 1980).	24
Figure 22 – Linear elastic stress fields normalized to remote stress σ_{rx} for lamina with $\bar{\phi} = 20^\circ$ in-plane waviness under uniaxial normal longitudinal loading: (a) normal longitudinal stress in local 1-direction σ_{11} , (b) normal transverse stress in local 2-direction σ_{22} , (c) local in-plane shear stress in 12-direction σ_{12} , and (d) local coordinate axes.	26
Figure 23 – Displacement in x-direction for a tensile loaded model plotted on undeformed shape: (a) lamina with no defect, (b) lamina with $\bar{\phi} = 20^\circ$ in-plane central waviness.	27
Figure 24 – Maximum normalized stresses for uniaxially longitudinal loaded laminae as a function of peak misalignment angle ($\bar{\phi}$).	28
Figure 25 – Hashin critical failure indices for a lamina with $\bar{\phi} = 20^\circ$ in-plane central waviness at initial failure: (a) Matrix compression index for a lamina under longitudinal compression; (b) Matrix tension index for a lamina under longitudinal tension.	28
Figure 26 – (a) Longitudinal tensile and (b) longitudinal compressive initial failure strength ratio of the lamina with central waviness normalized with respect to the lamina with no defect.	29
Figure 27 – Linear elastic stress fields normalized to remote stress σ_{ry} , for $\bar{\phi} = 20^\circ$ in-plane waviness under uniaxial normal transverse loading: (a) normal longitudinal stress in local 1-direction σ_{11} , (b) normal transverse stress in local 2-direction σ_{22} , (c) local in-plane shear stress in 12-direction σ_{12} , and (d) local coordinate axes.	30
Figure 28 – Maximum normalized stresses for uniaxially transverse loaded laminae as a function of peak misalignment angle ($\bar{\phi}$).	31
Figure 29 – Hashin critical failure indices for a lamina with $\bar{\phi} = 20^\circ$ in-plane central waviness at initial failure: (a) Matrix compression index for a lamina under transverse compression; (b) Matrix tension index for a lamina under transverse tension.	32

Figure 30 – (a) Transverse tensile and (b) transverse compressive initial failure strength ratio of the lamina with central waviness normalized with respect to the lamina with no defect. ...	32
Figure 31 – Legend for load case identification of Figure 32Figure 37.....	33
Figure 32 – Normal longitudinal stress in local 1-direction (σ_{11}) for a lamina with $\bar{\phi} = 20^\circ$ in-plane waviness, under uniaxial and biaxial responses.....	34
Figure 33 – Normal transverse stress in local 2-direction (σ_{22}) for a lamina with $\bar{\phi} = 20^\circ$ in-plane waviness, under uniaxial and biaxial responses.....	35
Figure 34 – In-plane shear stress in local 12-direction (σ_{12}) for a lamina with $\bar{\phi} = 20^\circ$ in-plane waviness, under uniaxial and biaxial responses.	36
Figure 35 – Hashin critical failure indices for a lamina with $\bar{\phi} = 20^\circ$ in-plane waviness at initial failure, under uniaxial and biaxial responses. Matrix compression index for load cases (iv), (vi), (vii) and (viii); Matrix tension index for load cases (i), (ii), (iii) and (v).	37
Figure 36 – Initial biaxial failure strain ratio of laminae with central waviness normalized with respect to laminae with no defect.	38
Figure 37 – Linear elastic stress fields normalized to remote stress σ_{rx} for lamina with $\bar{\phi} = 40^\circ$ in-plane waviness under uniaxial normal longitudinal loading: (a) normal longitudinal stress in local 1-direction σ_{11} , (b) normal transverse stress in local 2-direction σ_{22} , (c) local in-plane shear stress in 12-direction σ_{12} , and (d) local coordinate axes.....	44
Figure 38 – Hashin critical failure indices for a lamina with $\bar{\phi} = 40^\circ$ in-plane central waviness at initial failure: (a) Matrix compression index for a lamina under longitudinal compression; (b) Matrix tension index for a lamina under longitudinal tension.....	45
Figure 39 – Linear elastic stress fields normalized to remote stress σ_{rx} for lamina with $\bar{\phi} = 5^\circ$ in-plane waviness under uniaxial normal longitudinal loading: (a) normal longitudinal stress in local 1-direction σ_{11} , (b) normal transverse stress in local 2-direction σ_{22} , (c) local in-plane shear stress in 12-direction σ_{12} , and (d) local coordinate axes.....	45
Figure 40 – Hashin critical failure indices for a lamina with $\bar{\phi} = 5^\circ$ in-plane central waviness at initial failure: (a) Matrix compression index for a lamina under longitudinal compression; (b) Matrix tension index for a lamina under longitudinal tension.....	46
Figure 41 – Linear elastic stress fields normalized to remote stress σ_{ry} for lamina with $\bar{\phi} = 40^\circ$ in-plane waviness under uniaxial normal transverse loading: (a) normal longitudinal stress in local 1-direction σ_{11} , (b) normal transverse stress in local 2-direction σ_{22} , (c) local in-plane shear stress in 12-direction σ_{12} , and (d) local coordinate axes.....	47

Figure 42 – Hashin critical failure indices for a lamina with $\bar{\phi} = 40^\circ$ in-plane central waviness at initial failure: (a) Matrix compression index for a lamina under transverse compression; (b) Matrix tension index for a lamina under transverse tension.....	48
Figure 43 – Linear elastic stress fields normalized to remote stress σ_{ry} for lamina with $\bar{\phi} = 5^\circ$ in-plane waviness under uniaxial normal transverse loading: (a) normal longitudinal stress in local 1-direction σ_{11} , (b) normal transverse stress in local 2-direction σ_{22} , (c) local in-plane shear stress in 12-direction σ_{12} , and (d) local coordinate axes.....	48
Figure 44 – Hashin critical failure indices for a lamina with $\bar{\phi} = 5^\circ$ in-plane central waviness at initial failure: (a) Matrix compression index for a lamina under transverse compression; (b) Matrix tension index for a lamina under transverse tension.....	49

LIST OF TABLES

Table 1 - Elastic mechanical properties of unidirectional carbon/epoxy lamina (AS4/3501-6) (DANIEL and ISHAI, 1994)	21
Table 2 - Allowable stresses of the unidirectional carbon/epoxy (AS4/3501-6) (DANIEL and ISHAI, 1994)	24
Table 3 - Apparent elastic axial modulus (E_{1w}) at different values of peak misalignment angle ($\bar{\phi}$).....	25
Table 4 - Apparent elastic transverse modulus (E_{2w}) at different values of peak misalignment angle ($\bar{\phi}$).	29
Table 5 – Critical Hashin failure criterion index composition for a lamina with $\bar{\phi} = 40^\circ$ in-plane central waviness, under uniaxial and biaxial responses.....	50
Table 6 – Critical Hashin failure criterion index composition for a lamina with $\bar{\phi} = 20^\circ$ in-plane central waviness, under uniaxial and biaxial responses.....	50
Table 7 – Critical Hashin failure criterion index composition for a lamina with $\bar{\phi} = 5^\circ$ in-plane central waviness, under uniaxial and biaxial responses.....	51

LIST OF NOMENCLATURE

123 – Local coordinate system

xyz – Global coordinate system

L – Lamina total length

l – Wavy region length

H – Lamina total height

h – Wavy region height

$u(x)$ – Displacement in global x-direction

$u(y)$ – Displacement in global y-direction

ϕ – Misalignment angle

$\bar{\phi}$ – Peak misalignment angle

δ – Wave amplitude

λ – Wavelength

E_1 – Longitudinal modulus (in local 1-direction)

E_{1w} – Apparent longitudinal modulus (in global x-direction) for a lamina with waviness

E_2 – Transverse modulus (in local 2-direction)

E_{2w} – Apparent transverse modulus (in global y-direction) for a lamina with waviness

G_{12} – Shear modulus

ν_{12} – Poisson's ratio associated with loading in the 1-direction and strain in the 2-direction

F_{1t} – Longitudinal tensile strength

F_{1c} – Longitudinal compressive strength

F_{2t} – Transverse tensile strength

F_{2c} – Transverse compressive strength

S_t – Longitudinal shear strength

S_1 – Transverse shear strength

α - Coefficient of shear stress contribution to fiber tensile criterion of Hashin Initiation Criterion

σ_{11} – Longitudinal normal stress

σ_{22} – Transverse normal stress

σ_{12} – In-plane shear stress

σ_{rx} – Remote applied longitudinal stress

σ_{ry} – Remote applied transverse stress

σ_0 – Biaxial normal stress

LIST OF ACRONYMS

CFRP – Carbon fiber reinforced plastic

HFC – Hashin failure criterion

FEA – Finite Element Analysis

FEM – Finite Element Method

HDF – Hot Drape Forming

RVE – Representative Volume Element

SF – Severity Factor

FW – Fiber waviness

RTM – Resin transfer molding

1

INTRODUCTION

1.1 Background

Advanced composites are widely used in aerospace industries due to their higher specific properties and their elastic tailoring ability. Composites application has improved in such a way that, prior to the mid-1990s, composites were mainly limited to use in secondary structures, but with the development of Airbus 380, Boeing 787 and Lockheed Martin F-22 e F-35, composites are now being extensively utilized in primary structures such as wings and fuselage components (ABOUDI *et al.*, 2012).

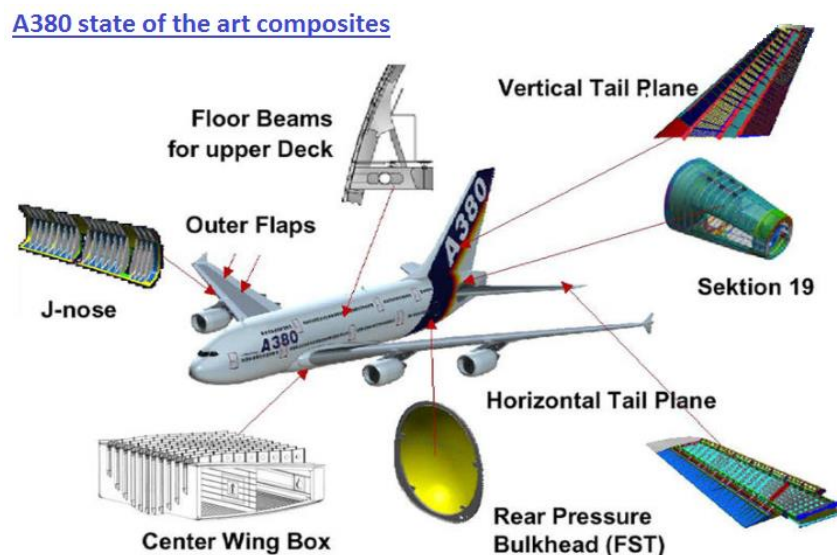


Figure 1 – Major carbon fiber reinforced plastic (CFRP) and thermoplastics application in AIRBUS A380

(<https://composite.wordpress.com/>)

The design of composite materials has its particularities as it differs from conventional metallic isotropy design due to the existence of material inhomogeneity and inherent anisotropy. Furthermore there is a hierarchy of structures in the material, i.e. a variety of scales that can be perceived and that defines the modeling and the analysis approach.

Composites need then to be understood at different levels of measurement, ranging from the constituent (fiber, inclusion, matrix and interface) to the real-scale structure. However, when trying to predict damage and failure mechanisms, the mechanics of these phenomena is only captured at the constituent scale, where they are actually occurring.

Particularly for aerospace applications, design for damage tolerance must account for the presence of flaws in the structure that will result in a structural performance reduction. These flaws may be generated during manufacturing stages (named defects) or during operation life (damages). Thus there is a need to investigate the effects associated with these anomalies in the field of composite applications.

1.2 Objectives

This dissertation aims to study the effect of in-plane fiber waviness in unidirectional carbon reinforced plastic (CFRP) composites under plane stress. Effects on key structural properties such as stiffness and strength were quantitatively evaluated through a FEM analysis-based methodology. Influence with regard to initial failure was evaluated, providing a computationally efficient framework to substantiate decisions in quality control, supporting accept/reject/repair decisions.

1.3 Justification

Fabrication processes always present a degree of variability that can often lead to defect occurrence, being fiber waviness one of the most frequent ones. It is important to understand how the presence of waviness affects structural performance by closer investigating the triggered failure modes under different load conditions. Conventional finite element analyses do not capture the local effects induced by this fiber misalignment condition.

1.4 Methodology

The work was divided into the following activities:

- Specific literature review regarding waviness causes, occurrence and detection level applied to aeronautic manufacturing;

- Investigation of state-of-the-art modeling to describe composite structures in the presence of fiber waviness;
- Development of numerical method to simulate laminae containing in-plane waviness under plane stress state, under uniaxial and biaxial loading. Abaqus® environment must be used;
- Automation of the FEM model generation by means of tool development using Python scripting for Abaqus®;
- Results analysis and comparison.

2

LITERATURE REVIEW

2.1 Variability and defects in composites

As production rates of advanced composites are expected to expand, there is a need to review the employed quality of materials, processes and design practices (POTTER, 2009). The fabrication quality control target must be zero defects, zero rework and repair and zero scrap. It is then vital to understand how design and process can influence the outcome of materials, by means of discussing potential sources of variability.

Incoming reinforcement and prepreg used for long fiber composite applications present intrinsic variability in mass/unit area, in the resin weight percentage and in average fiber straightness. Usually this variation in properties can be mainly linked to transportation/storage conditions and to stiffness and alignment of rollers used in the prepregging process. This material variability can generate non-conforming thickness in laminates, undesirable voids and even wrinkled areas.

It is essential to carefully detail the process drape strategy in order to control geometry distortions, avoiding localized folds and misalignments. Double curved surfaces can be a challenge and cause a high level of wrinkling. For this purpose, there are several draping simulation software packages designed to virtually prototype the layup of complex parts.

Variability can be traced to moulding processes aspects like consolidation and resin flow features. Deviations from designed part geometry are likely to occur in a phenomenon named fiber bridging, as presented in Figure 2. The main factors that lead to bridging are: tight design radius, stiff reinforcement and low coefficient of friction.

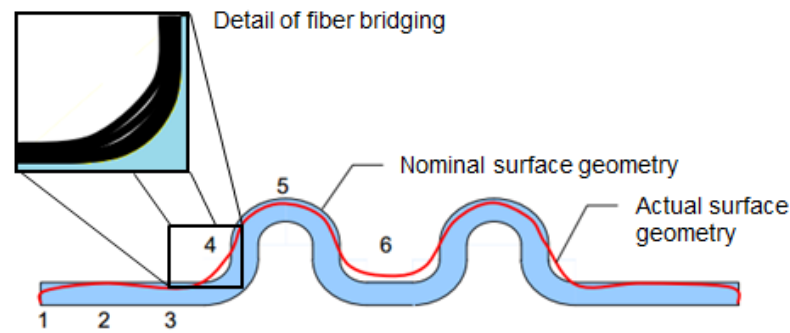


Figure 2 - Typical deviations from the designed part geometry (POTTER, 2009).

The cure process is also a source of variability, since it introduces residual stresses and thermal distortions provoked by different matrix and fiber in in-plane and through thickness expansion coefficients. Effects such as resin rich zones and constrained resin shrinkage can likewise appear. The regions of greatest complexity are the ones typically subjected to the most complex residual stress fields and where defects are most likely to take place.

Final fabrication stages such as machining, assembly, handling and even storage must also be properly executed, otherwise they can induce variations in the final part quality. Therefore a successful composite manufacturing can only be achieved by a combination of decisions in design stages, specific manufacture planning and careful control of materials and process variability. Figure 3 visually displays several potential causes of variability and defects in composites.

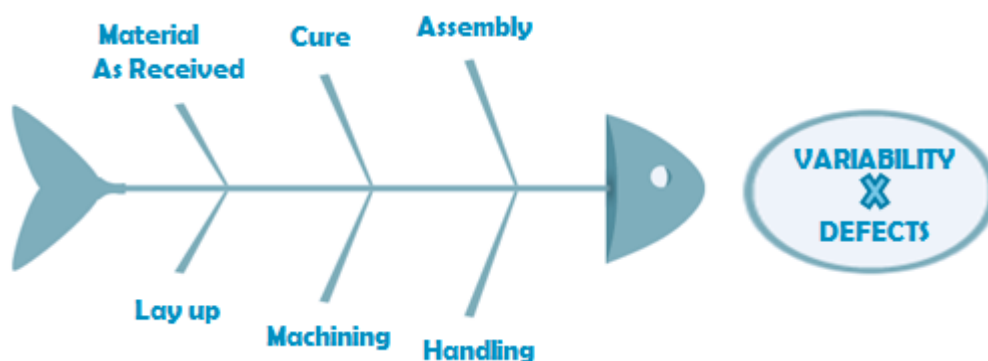


Figure 3 – Cause and effect diagram of variability and defects in composite materials.

Once that variation is present in the output of every fabrication process, it is then important to state at what point a feature becomes a defect. In the context of structure manufacturing, defect can be defined as an imperfection which exceeds a geometrical tolerance, presents a

reduced structural performance or in some other way fails to meet the design specifications and acceptance criteria.

2.2 Waviness

2.2.1 General aspects

In practice, composite structures can be subjected to several types of defects generated during manufacturing. Fiber waviness is one geometrical defect type characterized by fiber misalignment of an otherwise straight ply or group of plies. Some of the available literature (FARNAND, 2016; HALLANDER *et al.*, 2013) makes a distinction between the terms “waviness” and “wrinkling” according to the defect occurrence plane: the former refers to defects in-plane while the latter alludes to out-of-plane alterations. This work adopts the term “waviness” for both occurrence planes, as also performed by several authors (SUTCLIFFE *et al.*, 2012; KARAMI and GARNICH, 2005; MIZUKAMI *et al.*, 2015). Figure 4 presents a sketch of both in and out-of-plane waviness and micrograph pictures of real encountered defects.

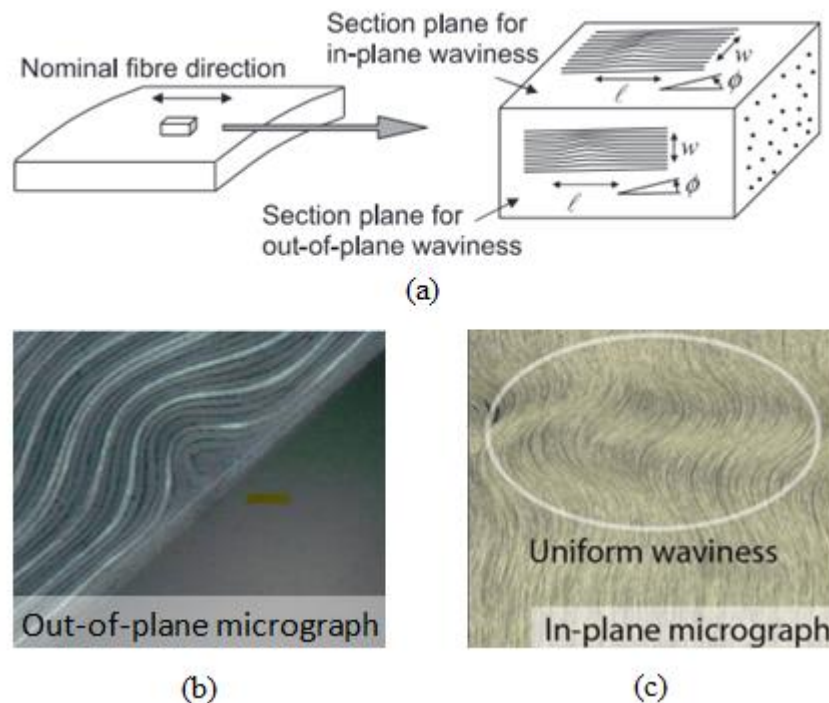


Figure 4 – (a) In and out-of-plane waviness configuration (SUTCLIFFE *et al.*, 2012); (b) Out-of-plane waviness from cut micrograph (HALLANDER *et al.*, 2013); (c) In-plane waviness from surface micrograph (FARNAND, 2016)

In order to describe waviness morphology, the wave shape can be approximate to a sinusoidal curve (CIMINI JR, 1997) or even a Gaussian function (SHAMS and ELHAJJAR, 2015) for modelling intentions. Waviness is characterized by amplitude and wavelength, its most important parameters.

The wavelength of waviness defects varies in size from a few millimeters, when it matches tow or ply dimensions, to some centimeters, when they provide truly weak points for the structure (LEMANSKI and SUTCLIFFE, 2012). Regarding defect spatial distribution, waviness can be randomly distributed across the structural part or it can be localized, restricted to a small portion of the structure.

Out-of-plane waviness has been investigated in depth (CAIAZZO *et al.*, 2000; SHAMS and ELHAJJAR, 2015; ALTMANN *et al.*, 2015), while in-plane waviness studies are not so frequent. This work will then focus on in-plane defects. Three sections of composites containing different configurations of in-plane fiber waviness are shown in Figure 5.

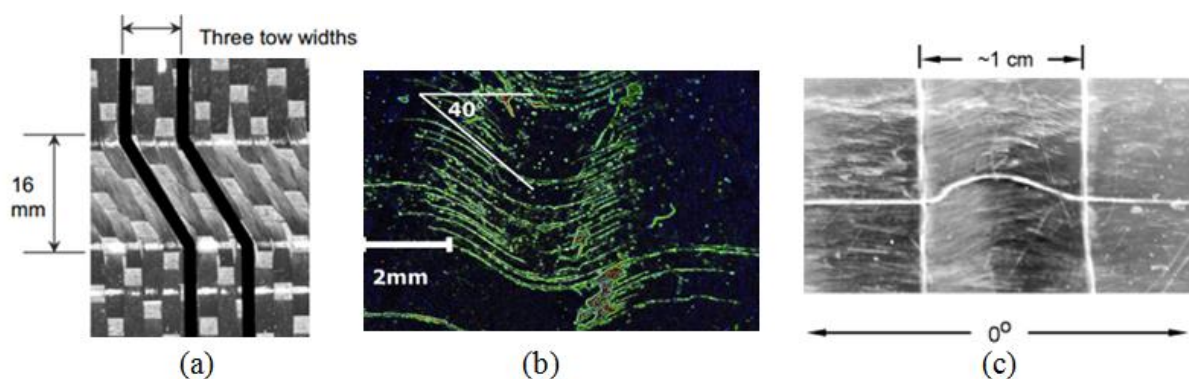


Figure 5 – (a) In-plane waviness in a fabric specimen (POTTER, 2009); (b) In-plane waviness in unidirectional material processed by RTM (POTTER, 2009); (c) In-plane waviness in a single-ply laminate of Carbon/Epoxy processed by RTM (MANDELL *et al.*, 2012).

The detection and measurement of waviness in situ can be challenging, especially for cases of embedded defects. Several techniques are available and new ones are being developed. The first attempts consisted of sectioning methods that used the fibers elliptical cross section when cut on an oblique plane to estimate fiber orientation (YURGATIS, 1987). Technology improvement has allowed the appearance of non-destructive and automated techniques, such as X-ray computed tomography (SALABERGER *et al.*, 2011), ultrasonic array scattering data (PAIN and DRINKWATER, 2013) and near infrared hyperspectral imaging method (ELHAJJAR *et al.*, 2016). The latter is based on the identification of resin rich areas, which is

an indicator of waviness, providing a 3D profile of resin features, illustrated in a defect map (Figure 6).

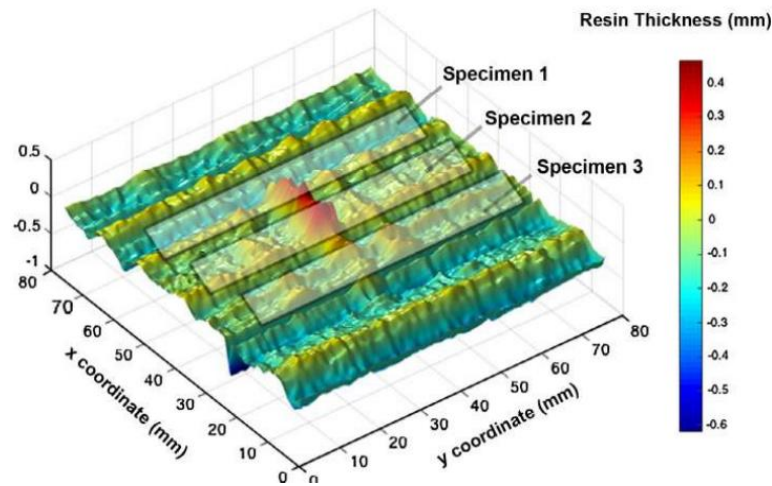


Figure 6 - 3D surface map of distributed resin pockets measured by near infrared hyperspectral imaging method (ELHAJJAR *et al.*, 2016)

One relevant aspect of waviness investigation is how to produce size controlled ply waviness profiles in laboratory for further experimentation. Several fabrication techniques have been developed and reported in the literature. ELHAJJAR *et al.* (2016) have highlighted the use of ply drop offs and transverse strips of composite material to trigger the out-of-plane waviness profile, the utilization of metallic rods to initiate wrinkling and the use of oversized prepreg plies in conforming to a given geometry.

CHAKRAPANI *et al.* (2014) have fabricated samples with discrete in-plane waviness in glass fiber/epoxy laminates, in order to develop a Lamb wave detection and characterization technique for in-plane defects. A sheet of dry glass fiber is inserted in the setup described in Figure 7 and the two fixed cylinders are clamped down, thus fixing the fabric in 1-direction. Next, the center cylinder is moved by a known amount, shearing the fabric in the 1-2 plane.

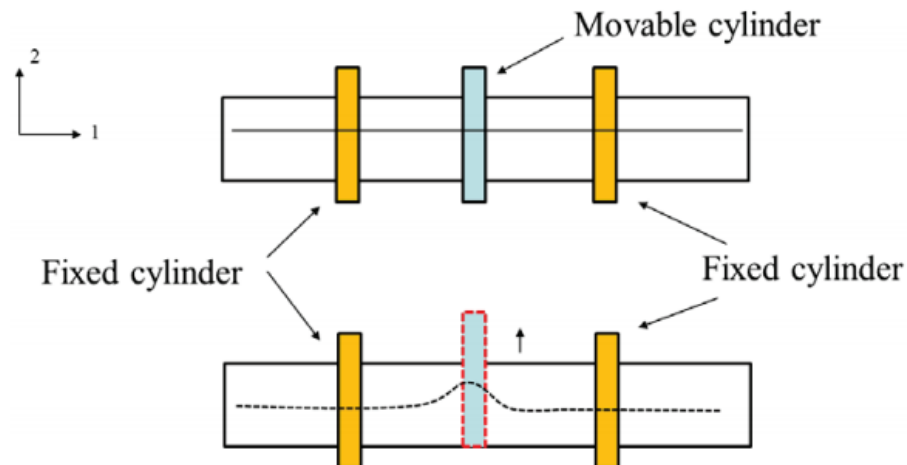


Figure 7 – Schematic of the fabrication method to create in-plane waviness. The movable cylinder can translate in the 2-direction, while the fixed cylinders can't move (CHAKRAPANI *et al.*, 2014)

MIZUKAMI *et al.* (2016) have developed an experimental method to facilitate the generation of in-plane fiber waviness in probes used to detect and characterize fiber orientations using eddy current testing. As schematically described in Figure 8, CFRP prepregs were stacked on an aluminum plate and the resin at the center of the lamina was removed by wiping it with a paper towel soaked with acetone. By removing transversal fiber support, fibers can then deform. Prepregs were sandwiched between aluminum plates and vacuum pressure was applied.

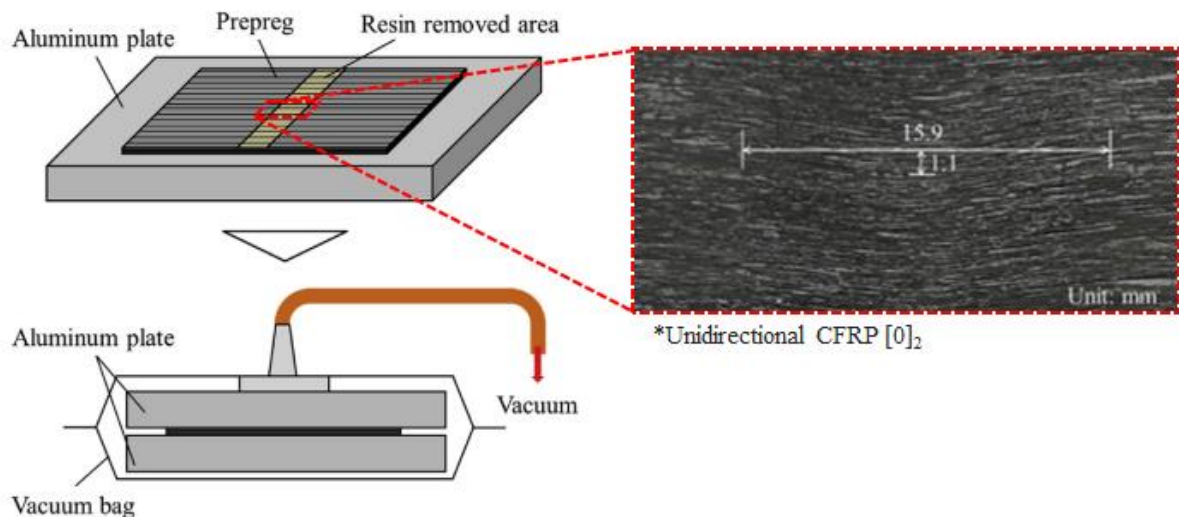


Figure 8 – Method used to fabricate a specimen with in-plane FW and photograph of the induced defect (adapted from MIZUKAMI *et al.*, 2016)

2.2.2 Manufacturing aspects

Waviness occurrence is normally linked to the following main causes: non uniform pressure from other composite layer or wrinkles in bagging, residual stresses due to tooling or when different layers of materials are co-cured in differing configurations (POTTER *et al.*, 2008). KUGLER and MOON (2002) have also identified cooling rate, tool plate material and length of cure as processing parameters that can also lead to the development of waviness defects in laminates.

It is important to highlight that, in composites manufactured by hand layup, defects are most likely to appear. When it comes to industrial composite components manufactured with elevated level of automation, waviness is commonly found in filament wound cylindrical structures, in flat thick laminates and in complex RTM (Resin transfer molding) parts (CIMINI JR, 1997). Another composite manufacturing process that can lead to fiber waviness is the Hot Drape Forming (HDF), which is used for aerospace components building, such as wing spars (HALLANDER *et al.*, 2013). Improper tensioning during pultrusion may also be a cause for process-induced waviness (MALLICK, 1997).

2.2.3 Waviness forming mechanism

In order to be able to avoid waviness development, it is of vital importance to understand the forming mechanisms of these defects. Such mechanisms occur in a simultaneous manner and are a consequence of the interaction between forming forces and directions determined by the part geometry, combined with material properties and stacking sequence. Intraply and interply shear, ply bending, intraply axial loading and compaction/consolidation are material/process specificities that play a significant role in the forming outcome (HALLANDER *et al.*, 2013).

SJÖLANDER *et al.* (2016) have performed an experimental/simulation study of waviness development during forming of a multi-layer prepreg spar with a recess area. The authors have identified that, when forming a stack onto a double curvature geometry, the laminate experiences a relaxation process, undergoing in-plane deformation that normally occurs by shear or normal strain. If there is not enough deformation, waviness occurs. The lack of mobility of the stack can then generate two different forming cases:

- **GLOBAL COMPRESSION:**

A general mechanism for all materials, it is caused by excess length that is then collected in a wrinkle. For laminates, it appears when the whole stack is under compression, resulting in buckling of the entire region. This phenomenon happens when a stack is formed over a convex geometry, for instance.

- **LOCAL COMPRESSION:**

This mechanism appears when a single layer with a specific fiber direction is under compression, undergoes buckling and the deformation then propagates through the stack. When the direction of the stress is aligned with the fiber direction, axial stress (either tensile or compressive) in the fiber will be created.

When investigating defect occurrence in forming C-channels of carbon-epoxy prepregs, FARNAND (2016) has detected that several out-of-plane waviness externally visible after forming disappeared after cure. That was explained by a conversion mechanism which turned out-of-plane waviness into in-plane misalignment and was attributed to curing bag tension. The identified post-form out-of-plane to in-plane waviness conversion mechanism provides reasons to improve understanding of mechanical performance effects from waviness, which is the subject of this dissertation.

2.3 Bibliographic Review

2.3.1 The contribution of Hsiao and Daniel

HSIAO and DANIEL (1996) investigated the effect of fiber waviness on stiffness and strength reduction of thick unidirectional composites under compressive loading.

They have developed an analytical model to determinate the effective elastic properties as a function of fiber waviness, assumed with an initial deflection sinusoidally curved, as showed in Figure 9. Stresses and strains were obtained using Classical Lamination Theory associated with incremental analysis. Local ply failure was predicted using Tsai-Wu criterion.

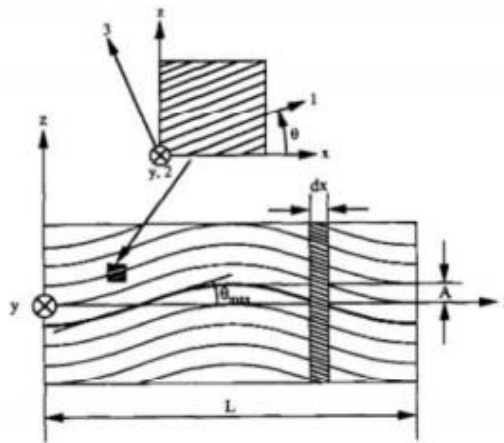


Figure 9 - Representative volume and coordinates for a unidirectional composite with uniform waviness (HISAO and DANIEL, 1996)

Techniques using the cure of prepreg tapes wound around a mandrel were developed in order to fabricate thick specimens with controlled waviness. Compression tests on 1D laminates using strain gages and video photography were conducted on specimens with and without defects to verify the predictions.

Both major Young's modulus and compressive strength presented serious degradation as the fiber waviness increased. Carbon/epoxy material was shown to be much more sensitive to the defect than S-glass/epoxy material. The dominant failure mechanism was initiated by local interlaminar shear stress, followed by delamination and layer buckling.

2.3.2 The contribution of Cimini Jr

The work of CIMINI JR (1997) aimed to determine quantitatively the effect of out-of-plane ply waviness on the in-plane stiffness of composite laminates. A mathematical model was proposed to capture the local mechanical behavior of regions in the presence of fiber misalignment. Defects were described as in-phase sine-waves and uniform and graded embedded waviness were simulated, varying its Severity Factor (the ratio between the amplitude of waviness and its wave-length).

In order to obtain the orientation of fibers in space, two coordinate systems transformation were necessary and the effective stiffness was calculated using both weighted average and spring-in-series approaches, as seen in Figure 10.

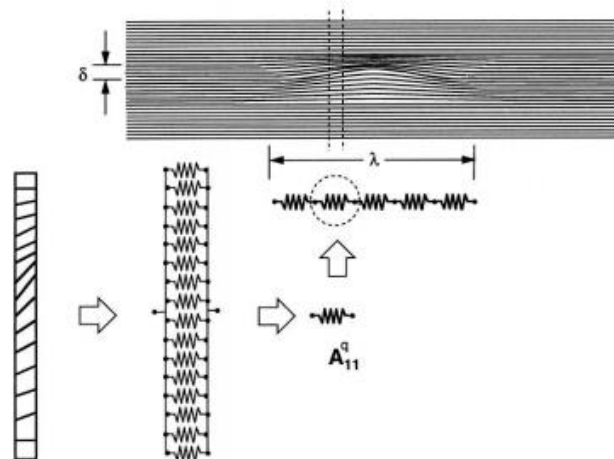


Figure 10 – Springs-in-series approach (CIMINI JR, 1997).

Model predictions were compared to test results and literature available data for unidirectional and cross-ply specimens with different lay-ups and materials. Influence parameters such as ply orientation and relative waviness area were also investigated.

The drop of properties was shown to be more significant in uniform embedded cases. In-plane stiffness was more affected for the 0° ply orientation laminates, with reductions as high as 50%, which indicates that extra careful is necessary when waviness occurs at plies aligned with load. S-glass/epoxy systems proved to not be as sensitive as the carbon/epoxy systems, the latter with a higher degree of anisotropy.

2.3.3 The contribution of Garnich and Karami

GARNICH and KARAMI (2004) have proposed a finite element formulation to simulate wavy fiber composites. They used a micromechanical model of a periodically unit cell consisting of unidirectional waved cylindrical fibers embedded within a matrix to determine average stress and strain components. This unit cell served as a three-dimensional Representative Volume Element (RVE) of a hexagonal packing arrangement.

Stress analyses were carried out for six independent load cases to determinate elastic stiffness parameters, whose evaluations were based on a volume averaging procedure over the whole volume of the unit cell. Simulations for several different fiber volume fractions as well as different amplitude to wavelength ratios were generated.

The results confirmed that waviness has a strong effect on stiffness, especially on the axial properties. The micromechanical model demonstrated the presence of local stresses that are not present in traditional structural macroanalysis and have a strong influence on composite strength. It must be pointed that the periodically boundary constraints employed simulated an idealized material with global uniform fiber waviness, a conservative scenario that is not likely to occur in practice and significantly overestimates the strength reduction.

In 2005 continuing the initiated work, KARAMI and GARNICH proposed the use of an equivalent kind of RVE, being modelled as a straight unit cell with wavy material orientation, with the purpose of simplifying the FEM analysis. The difference from the two RVE proposals can be seen in Figure 11.

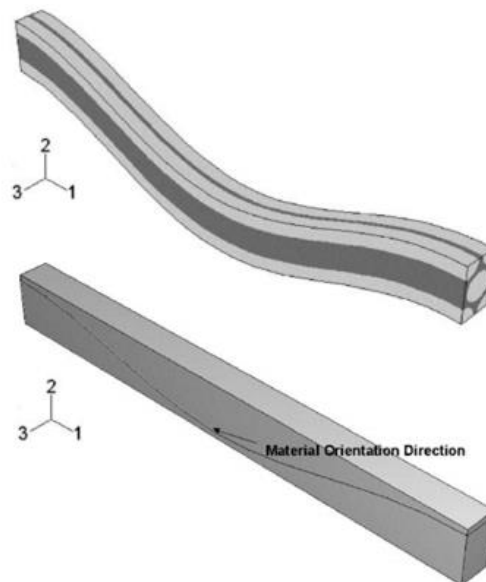


Figure 11 - A comparison between the three-dimensional wavy unit cell modelling and the straight unit cell with wavy material orientation (KARAMI and GARNICH, 2005)

Furthermore, differently from the first modeling approach where all plies were considered waved, it was simulated the constraining effects of localized wavy layers bonded between straight neighboring layers. Results showed that the added layers effectively increased laminate stiffness by inhibiting the fiber straightening mechanism and approximated the behavior with real encountered applications.

2.3.4 The contribution of Altmann *et al.*

Altmann *et al.* (2015) have analyzed the effect of ply waviness on the strength behavior of unidirectional laminates under compressive loading by means of an analytical method. They considered a sinusoidal, in-phase, global, out-of-plane waviness geometry with uniform and graded amplitudes. The approach was inspired by the work of HSIAO and DANIEL (1996), with a code being implemented in Matlab®. Puck failure criteria were used and the results were validated by HSIAO and DANIEL (1996) experimental tests.

As presented in Figure 12, results showed that, having very small waviness, fiber properties dominate the failure mechanism. As waviness increases, the matrix properties define the strength behavior.

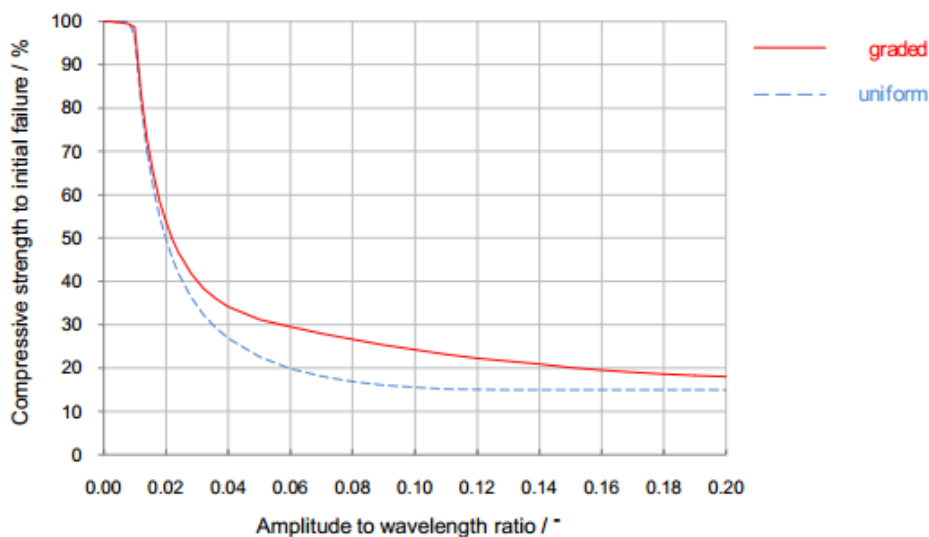


Figure 12 – Compressive strength of uniform and graded ply waviness (ALTMANN *et al.* 2015).

2.3.5 The contribution of Lemanski and Sutcliffe

LEMANSKI and SUTCLIFFE (2012) have studied via finite element analysis the effect of unidirectional composites with a region of misaligned fibers on the compressive behavior. In order to investigate the influence of fiber bending stiffness in microbuckle initiation, the material modeling followed two different approaches, both implemented using the commercial software Abaqus®:

- “Beam-and-shell” model: The geometry was represented by a mesh consisting of shell elements representing resin (Abaqus® element type S4) and beam elements

representing fiber reinforcement (Abaqus® element type B31). The second moment of area I of the beam introduced the bending stiffness of the fiber.

- “Rebar-and-solid” model: The geometry was represented by a mesh of 3D elements (Abaqus® element type C3D8I) with embedded unidirectional rebar reinforcement that did not include the effect of fiber bending. It consisted of a smaller model, easy to implement and quicker to solve.

Comparison of model approaches showed that, for waviness defects larger than about 200 times the fiber diameter, the additional compression due to bending stiffness is negligible.

Furthermore, the effect of various defect parameters was analyzed: initial misalignment angle, plate width covered by wavy path, length of wavy path on loading direction, position of wavy path relative to plate edge and wavy region in different layers of a laminate. Results showed that the compressive strength decreases rapidly with initial misalignment increase and with the increase of affected width proportion of ply. Effects of defect length and position relative to plate edge were less relevant and there was a strength reduction when waviness was extended through all layers.

Simulations of randomly distributed waviness were then performed in order to mimic the defect characterization found in RTM components (Figure 13).

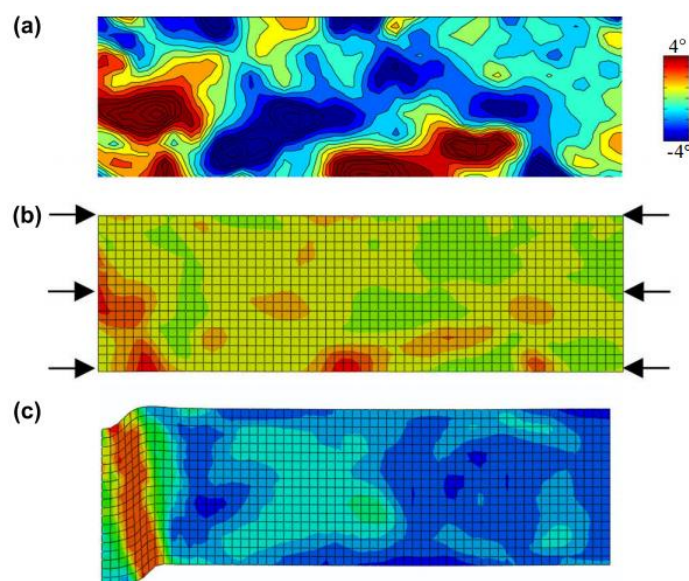


Figure 13 – Model of random waviness taken from RTM components: (a) initial misalignment angle; (b) von Mises stress distribution during elastic loading, (c) von Mises stress distribution after peak loading (LEMANSKI and SUTCLIFFE, 2012).

In summary, investigations proved that characterization of waviness defects in real structures needs to consider size and position of misaligned regions as well as the peak misalignment angle.

3

NUMERICAL APPROACH

3.1 Waviness geometry characterization

For the purpose of describing the intensity degree of the waviness defect, several authors have proposed the identification of parameters to characterize the defective region. By approximating fibers undulated shape to a sinusoidal curve (CIMINI JR and TSAI, 1999), a non-dimensional geometric parameter entitled Severity Factor (SF) was defined as the ratio between wave amplitude (δ) and length (λ), as shown in Figure 14 and represented by Equations (1) and (2).

Waviness severity has also been investigated as a function of the peak misalignment angle (LEMANSKI and SUTCLIFFE, 2012) and this will be the approach followed throughout this work. This characterization approach becomes advantageous because it is obtained by means of straight image examination of portions of the material. LEMANSKI and SUTCLIFFE (2012) have investigated the sensitivity of compressive strength to the misalignment angle of unidirectional composites with random distributed waviness. EDGREN and ASP (2005) have also used the maximum angle of misorientation to describe stiffness knock-down effects on non-crimp fabric composites. The identification of the peak misalignment angle ($\bar{\phi}$) parameter and its relation with wave amplitude and length are also presented in Figure 14 and Equation (3).

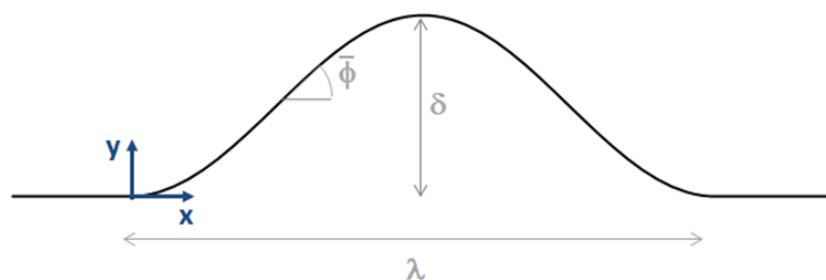


Figure 14 - Wave profile and its main geometric features.

$$y = \frac{\delta}{2} \cdot \left[1 + \sin\left(\frac{2\pi x}{\lambda} - \frac{\pi}{2}\right) \right] \quad (1)$$

$$SF = \frac{\delta}{\lambda} \quad (2)$$

$$\bar{\phi} = \tan^{-1}\left(\frac{\delta\pi}{\lambda}\right) \quad (3)$$

The problem was to investigate the implications of the presence of in-plane fiber waviness on a finite size unidirectional composite lamina. Waviness was represented as an embedded graded imperfection in order to resemble real defects. Model geometry was constructed as rectangular sheet of dimensions $L \times H$. The defective wavy region was confined to a central area of $l \times h$ dimensions so that, in all other sheet regions, the fibers remained straightly aligned. This approach avoids the extension of waviness to the edges, where it would lead to stress concentration and premature failure, approximating to defects found in sufficient large components.

In the wavy region, fibers are represented as in-phase sine-waves with the same wave length (λ). The amplitude of a central wave presents a maximum value (δ) while the amplitude of the adjacent waves decreases linearly from sheet center to the boundary of the wavy region where it reaches zero value, i.e, fibers become straight. This is shown in Figure 15.

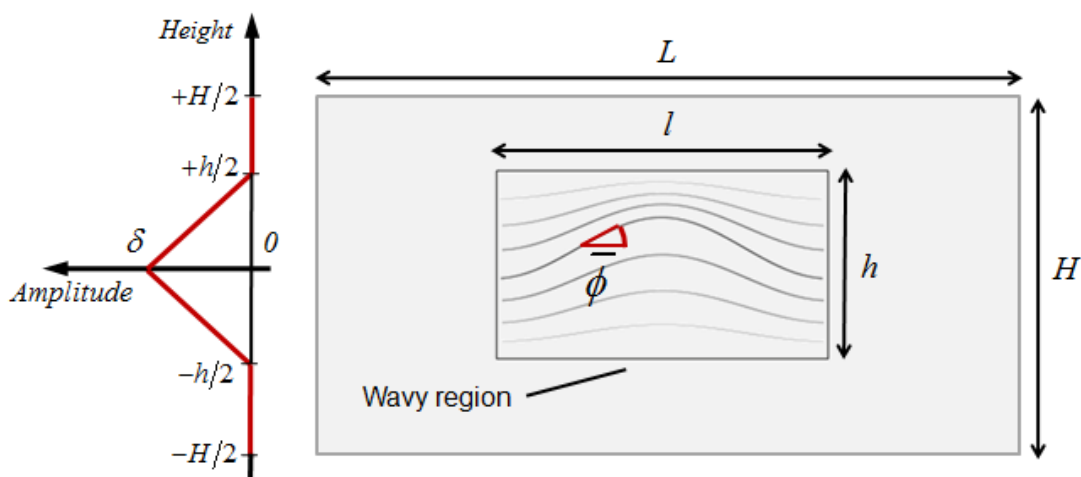


Figure 15 – Lamina parametric geometry.

Defect severity and its influence on failure behavior were investigated taking the peak misalignment angle ($\bar{\phi}$) as the sole influence parameter. Peak misalignment angles values

were considered as 5° , 20° and 40° , in order to simulate moderate, severe and very severe defects, respectively. All other lamina dimensions were taken as described in Equations (4)-(7) and the resulting geometries are presented in Figure 16.

$$l = \lambda \quad (4)$$

$$L = 2\lambda \quad (5)$$

$$h = 3\delta \quad (6)$$

$$\frac{H-h}{2} = \frac{\lambda}{2} \quad (7)$$

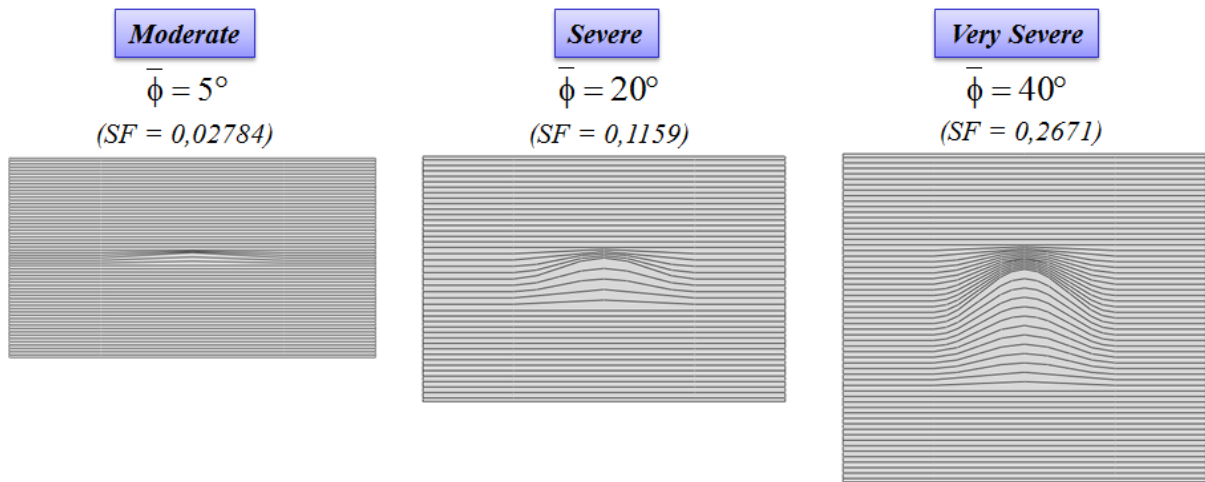


Figure 16 – Resulting geometries for the different severity of defects investigated.

3.2 Finite element modeling approach

Finite element modeling was performed using the commercial platform Abaqus®. Lamina geometry automated generation was accomplished by means of a plug-in specially built for this purpose, based on a parametric Python-scripting for Abaqus®.

A two-dimensional (2D) linear elastic analysis was developed. The examined material followed a plane stress assumption, considering stress components perpendicular to the lamina to be negligible. This is a valid approach since in most structural applications composite materials are used in the form of thin laminates loaded in the plane (DANIEL and ISHAI, 1994). Two-dimensional 4-node plane stress shell elements (Abaqus® element type CPS4R) were used. Mesh size was refined so that a sufficient fine mesh was able to resolve the sinusoidal variation and stress results converged. Figure 17 illustrates the mesh the $\bar{\phi} = 20^\circ$ model.

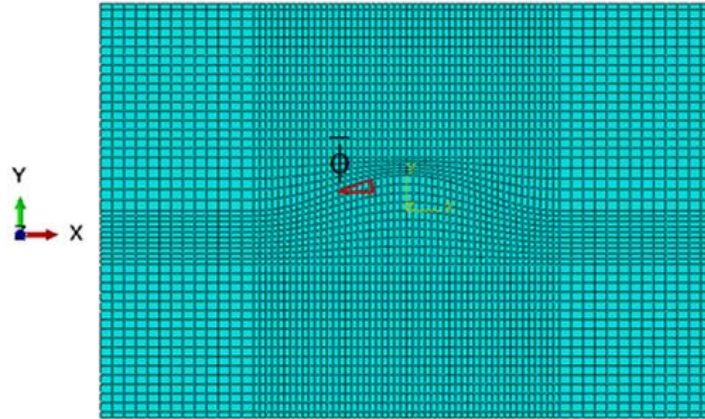


Figure 17 – FE element mesh (Lamina with $\bar{\phi} = 20^\circ$).

The analyzed material was a unidirectional carbon/epoxy composite (AS4/3501-6) and its orthotropic elastic stress properties in plane are summarized in Table 1.

Table 1 - Elastic mechanical properties of unidirectional carbon/epoxy lamina (AS4/3501-6) (DANIEL and ISHAI, 1994)

E_1 [GPa]	E_2 [GPa]	G_{12} [GPa]	ν_{12} [-]
142	10,3	7,2	0,27

Material was taken as a homogeneous media and fiber waviness orientation was accomplished by partitioning the sheet in a number of small regions across the height and assigning each region with a local orientation based on a sinusoidal curve. This was achieved by the use of Abaqus/CAE® “Discrete orientation”, which defines continually varying orientation that can follow the shape of a curve, as illustrated in Figure 18.

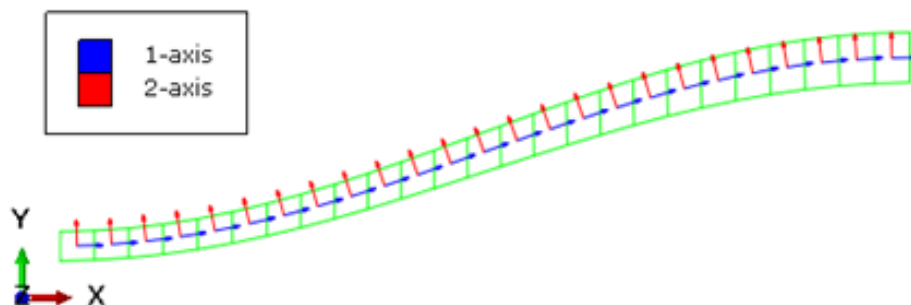


Figure 18 - Material orientation of a portion of the FE mesh. Local 1-axis points to fiber direction in agreement with wavy profile.

Lamina was subjected to three groups of in-plane load and boundary conditions: (a) Uniaxial normal longitudinal load; (b) Uniaxial normal transverse load; (c) Biaxial normal load. Simulations were divided into compressive and tensile loads, both applied as controlled prescribed displacements (u) on the edge opposite to the supported one, as sketched in Figure 19. For the biaxial response, all combinations of compressive and tensile loads in both longitudinal and transverse directions were taking into account. Figure 20 compiles all analyzed load cases.

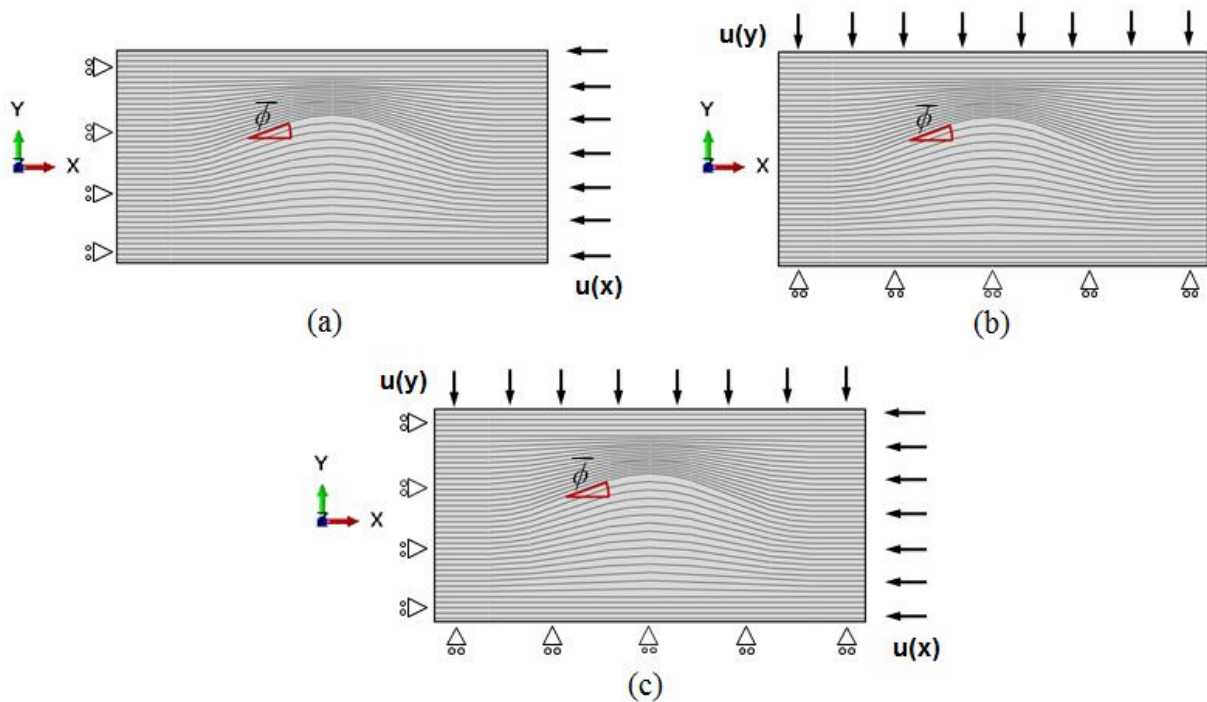


Figure 19 – Load and boundary conditions groups (for compressive cases): (a) lamina under uniaxial normal longitudinal load; (b) lamina under uniaxial normal transverse load; (c) lamina under biaxial normal loads.

For the biaxial loading, an initial simulation of a lamina with all fibers perfectly aligned (no waviness) was performed so that the generated stress state presents both normal longitudinal and transverse stresses with the same absolute value, i.e. $|\sigma_x| = |\sigma_y| = \sigma_0$. The applied displacement ratio (u_x/u_y) was obtained by plane stress state equations for an orthotropic material, using the elastic mechanical properties and sheet dimensions. This defined ratio of applied displacements, in the longitudinal and transverse directions, was then used as a prescribed displacement for the wavy lamina.


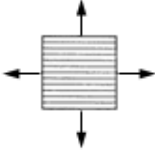

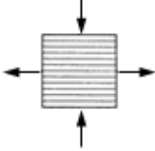

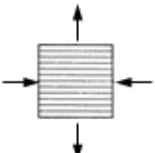

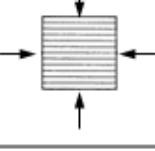
LOAD CASE	DESCRIPTION (ID)	LOAD CASE	DESCRIPTION (ID)
	Uniaxial Longitudinal Tension (T)		Biaxial Longitudinal Tension + Transverse Tension (T+Tt)
	Uniaxial Longitudinal Compression (C)		Biaxial Longitudinal Tension + Transverse Compression (T+Ct)
	Uniaxial Transverse Tension (Tt)		Biaxial Longitudinal Compression + Transverse Tension (C+Tt)
	Uniaxial Transverse Compression (Ct)		Biaxial Longitudinal Compression + Transverse Compression (C+Ct)

Figure 20 – Simulated load cases and corresponding text description and ID.

3.3 Failure Criteria

Hashin failure criterion (HFC) was used to predict damage initiation (HASHIN, 1980). HFC is a physically based criterion that captures the heterogeneous nature of the material, i.e., distinguishing between fiber and matrix failure. The first is governed by longitudinal stresses and the second is governed by transversal and tangential ones. This leads to four different failure indices with separate treatment of matrix and fibers. Equations (8)-(11) represent failure indices for Hashin under a plane stress state:

- Fiber tension ($\sigma_{11} > 0$):

$$IF_{ft}^2 = \left(\frac{\sigma_{11}}{F_{1t}} \right)^2 + \alpha \cdot \left(\frac{\sigma_{12}}{S_l} \right)^2 \quad (8)$$

- Fiber compression ($\sigma_{11} < 0$):

$$IF_{fc}^2 = \left(\frac{\sigma_{11}}{F_{1c}} \right)^2 \quad (9)$$

- Matrix tension ($\sigma_{22} > 0$):

$$(10)$$

$$IF_{mt}^2 = \left(\frac{\sigma_{22}}{F_{2t}} \right)^2 + \left(\frac{\sigma_{12}}{S_l} \right)^2$$

Matrix compression ($\sigma_{22} < 0$):

$$IF_{mc}^2 = \left(\frac{\sigma_{22}}{2S_t} \right)^2 + \left[\left(\frac{Y^C}{2S_t} \right)^2 - 1 \right] \cdot \frac{\sigma_{22}}{F_{2c}} + \left(\frac{\sigma_{12}}{S_l} \right)^2 \quad (11)$$

where F_{1t} and F_{1c} denotes longitudinal tensile and compressive strengths; F_{2t} and F_{2c} , transverse tensile and compressive strengths; S_l , longitudinal shear strength; S_t , transverse shear strength and α is a coefficient that determines shear stress contribution to the fiber tension initiation criterion. The failure modes in unidirectional fiber composites related to these strengths are presented in Figure 21. The allowable strength values adopted in this work are presented in Table 2. The present analysis take $\alpha = 0$ and $S_t = F_{2c}/2$.

Table 2 - Allowable stresses of the unidirectional carbon/epoxy (AS4/3501-6) (DANIEL and ISHAI, 1994)

F_{1t} [MPa]	F_{1c} [MPa]	F_{2t} [MPa]	F_{2c} [MPa]	S_l [MPa]
2280	1440	57	228	71

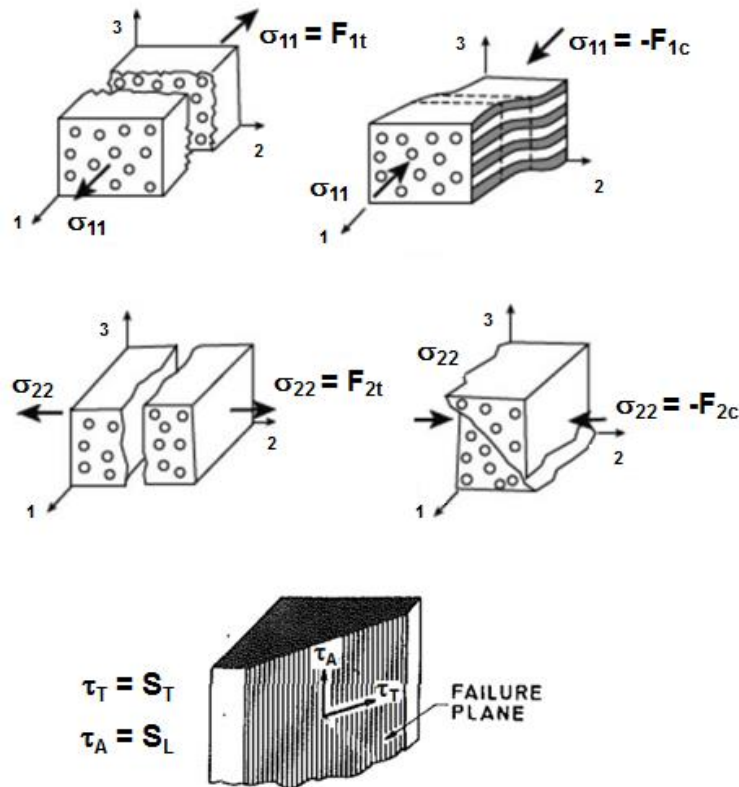


Figure 21 – Failure modes in unidirectional fiber composites (CARLSSON *et al.*, 2013; HASHIN, 1980).

4

RESULTS AND DISCUSSION

4.1 Uniaxial normal longitudinal loaded laminae

The apparent axial stiffness (E_{1w}) of laminae in the presence of in-plane waviness was obtained by Equations (12)-(14).

$$E_{1w} = \frac{(\sigma_{avg})_x}{(\varepsilon_{avg})_x} \quad (12)$$

$$(\sigma_{avg})_x = \frac{Total_Force}{Cross_sectional_area} = \frac{R_x}{H} \quad (13)$$

$$(\varepsilon_{avg})_x = \frac{End_displacement}{Specimen_length} = \frac{u_x}{L} \quad (14)$$

The results are summarized in Table 3 and show that the apparent elastic modulus is affected by the presence of in-plane fiber waviness, although moderate and even severe defects present little effect (less than 5%).

Table 3 - Apparent elastic axial modulus (E_{1w}) at different values of peak misalignment angle ($\bar{\phi}$).

Defect classification	E_{1w}/E_1
Moderate ($\bar{\phi} = 5^\circ$)	0,9991
Severe ($\bar{\phi} = 20^\circ$)	0,9678
Very severe ($\bar{\phi} = 40^\circ$)	0,8455

The presence of fiber waviness, however, proved to significantly alter the stress field surrounding the defect. Figure 22 presents contours of local plane stresses normalized to the remote applied longitudinal stress (σ_{rx}) for the $\bar{\phi} = 20^\circ$ model. This general behavior is observed in the analyses with different peak misalignment angles and is shown in “Appendice: Simulation detailed results – Stress distribution”. For a uniaxially longitudinal

loaded specimen, the modification of material orientation causes local stiffness changes and the occurrence of normal transverse and shear stresses. Note that, if no waviness is present, the maximum values were to be $\sigma_{11} = 1$ and $\sigma_{22} = \sigma_{12} = 0$.

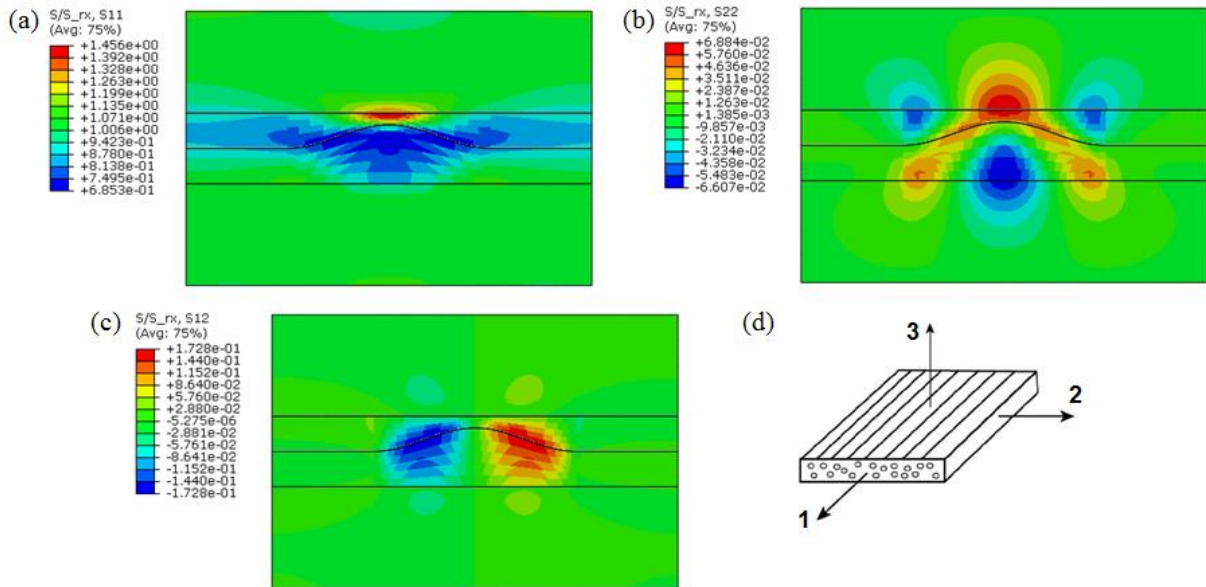


Figure 22 – Linear elastic stress fields normalized to remote stress σ_{rx} for lamina with $\bar{\phi} = 20^\circ$ in-plane waviness under uniaxial normal longitudinal loading: (a) normal longitudinal stress in local 1-direction σ_{11} , (b) normal transverse stress in local 2-direction σ_{22} , (c) local in-plane shear stress in 12-direction σ_{12} , and (d) local coordinate axes.

Results show a longitudinal stress concentration in the region right above the peak of the central wave, whilst the wavy region below presents longitudinal stress relaxation. This can be all related to local stiffness changes induced by fiber curvature.

In-plane waviness also induced the emergence of normal transverse stresses and in-plane shear stresses, following the patterns presented in Figure 22. These stresses are not present in traditional structural analyses which do not take fiber waviness into consideration and are usually unaccounted, although they provide implications to the failure mechanisms. The induced stresses are local anti-symmetric alterations, with no net effect at a global level.

Particularly for the shear stress cases, it can be identified an alternating positive and negative shear pattern around the peak misalignment angle positions. SJÖLANDER *et al.* (2016) have related this pattern as an indicator of waviness appearance when comparing forming FE-simulations with experimental forming studies, namely as “marcelling regions”.

Figure 23 compares the global x-displacement from a lamina with no waviness under longitudinal tension with a lamina in the presence of the defect. It can be seen that the strain experienced by the central part is transformed once that the waviness induces a reduction in axial stiffness.

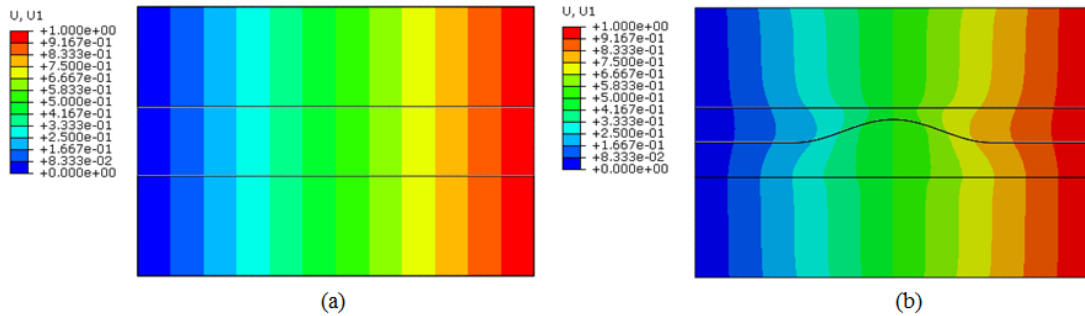


Figure 23 – Displacement in x-direction for a tensile loaded model plotted on undeformed shape: (a) lamina with no defect, (b) lamina with $\bar{\phi} = 20^\circ$ in-plane central waviness.

Maximum values of σ_{11} , σ_{22} and σ_{12} normalized to remote longitudinal uniaxial stress are summarized in Figure 24. Graphs indicate that the increase in misalignment angle provoked a trend for increase in maximum stresses, following an approximately linear relationship for both normal longitudinal and transverse stresses and an approximately quadratic relationship for shear stress. The order of magnitude varies according to the nature of the stress in question: while normal longitudinal stresses may experience a larger variation, the smaller variation of shear stresses will be significant in terms of failure, once that its allowable values are much lower (around 20 times lower for compressive strength, 32 times for tensile).

Analysis of HFC indices proved that failure will be initiated by matrix compression index for compressive loading, as presented in Figure 25(a). For tensile loading, matrix tension index will be the trigger for failure (Figure 25(b)). Failure is mainly dominated by shear stresses, as detailed in “Appendice: Simulation detailed results – Critical HFC index examination”, and its initiation point is localized in regions with maximum fiber inclination.

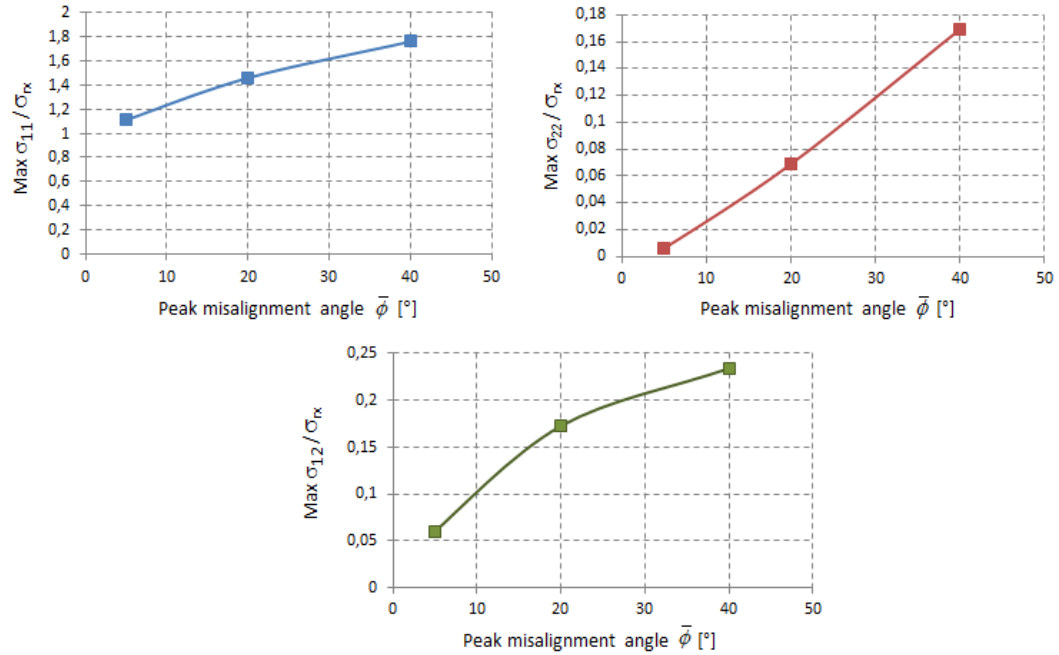


Figure 24 – Maximum normalized stresses for uniaxially longitudinal loaded laminae as a function of peak misalignment angle ($\bar{\phi}$).

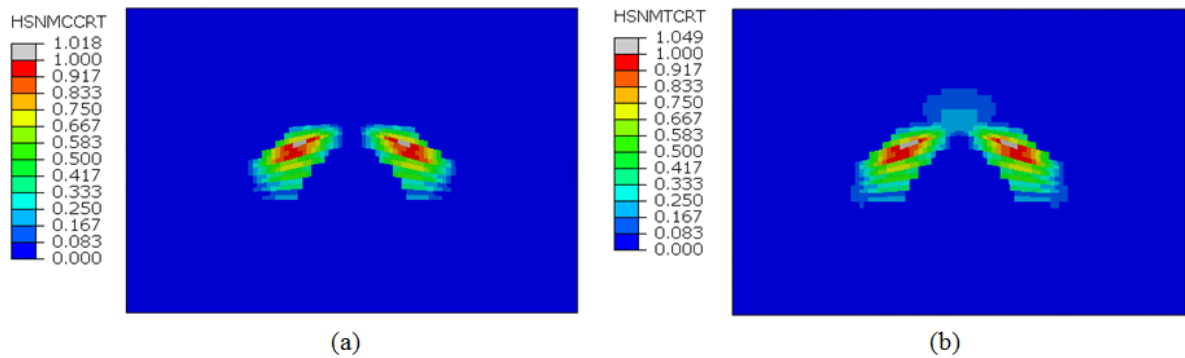


Figure 25 – Hashin critical failure indices for a lamina with $\bar{\phi} = 20^\circ$ in-plane central waviness at initial failure: (a) Matrix compression index for a lamina under longitudinal compression; (b) Matrix tension index for a lamina under longitudinal tension.

Figure 26 shows the strength reduction at initial failure influenced by the peak misalignment angle. The results, separated for tensile and compressive cases, are presented as a percentage ratio of the strengths of the lamina with central waviness normalized with respect to the lamina with perfectly straight and aligned fibers. Similar responses were found by ALTMANN *et al.* (2015) when investigating the degradation of mechanical properties of unidirectional laminae containing out-of-plane waviness using analytical and numerical models. Small waviness regions have failure dominated by fiber strength. As peak

misalignment angle increases, a different mode of failure is triggered and matrix properties dominate the strength behavior.

When comparing the apparent stiffness reduction with the strength knock-down, the lamina strength appears to be more sensitive to peak misalignment angle increase.

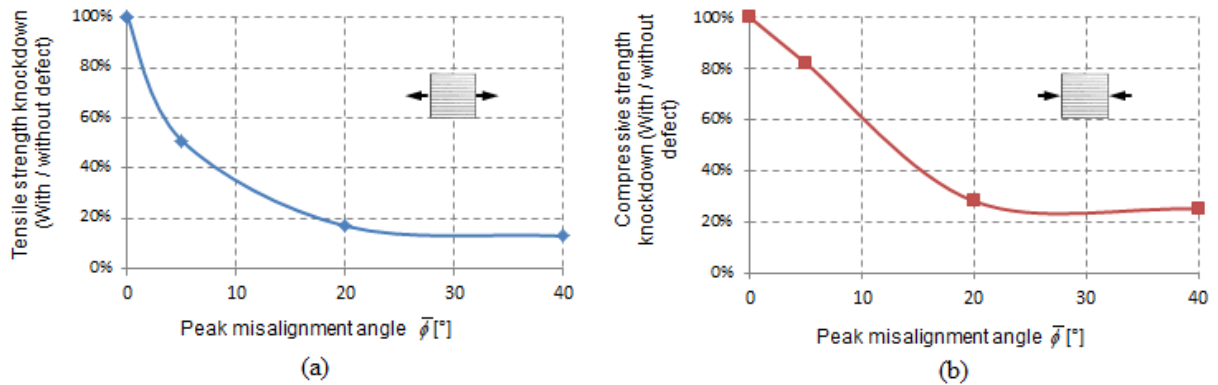


Figure 26 – (a) Longitudinal tensile and (b) longitudinal compressive initial failure strength ratio of the lamina with central waviness normalized with respect to the lamina with no defect.

4.2 Uniaxial normal transverse loaded laminae

The apparent transverse stiffness (E_{2w}) of laminae in the presence of in-plane waviness was obtained by Equations (15)-(17), in a similar manner to the longitudinal loading approach.

$$E_{2w} = \frac{(\sigma_{avg})_y}{(\varepsilon_{avg})_y} \quad (15)$$

$$(\sigma_{avg})_y = \frac{Total_Force}{Cross-sectional_area} = \frac{R_y}{L} \quad (16)$$

$$(\varepsilon_{avg})_y = \frac{End_displacement}{Specimen_length} = \frac{u_y}{H} \quad (17)$$

The results are summarized in Table 4 and show that effect of the defect in the apparent transverse elastic modulus is negligible.

Table 4 - Apparent elastic transverse modulus (E_{2w}) at different values of peak misalignment angle ($\bar{\phi}$).

Defect classification	E_{2w}/E_2
Moderate ($\bar{\phi} = 5^\circ$)	1,0001
Severe ($\bar{\phi} = 20^\circ$)	1,0030
Very severe ($\bar{\phi} = 40^\circ$)	1,0223

Analogously to the longitudinal load cases, the stress field surrounding the waviness defect is also modified. Figure 27 shows contours of local plane stresses normalized to the remote applied transverse stress (σ_{ry}) for $\bar{\phi} = 20^\circ$ model. Normal longitudinal and in-plane shear stresses are this time induced - if no waviness is present, the maximum values were to be $\sigma_{22} = 1$ and $\sigma_{11} = \sigma_{12} = 0$. Once again, the “marcelling region” pattern is observed in shear stresses distribution. Contours of laminae with different peak misalignment angles are presented in “Appendix: Simulation detailed results – Stress distribution”.

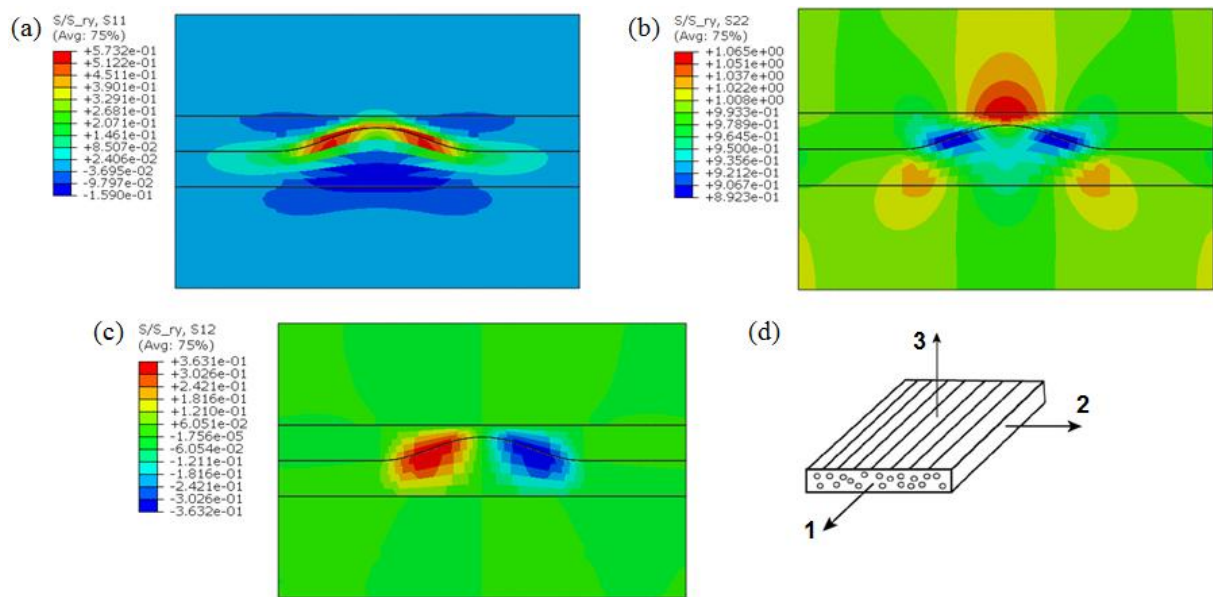


Figure 27 – Linear elastic stress fields normalized to remote stress σ_{ry} , for $\bar{\phi} = 20^\circ$ in-plane waviness under uniaxial normal transverse loading: (a) normal longitudinal stress in local 1-direction σ_{11} , (b) normal transverse stress in local 2-direction σ_{22} , (c) local in-plane shear stress in 12-direction σ_{12} , and (d) local coordinate axes.

Maximum values of σ_{11} , σ_{22} and σ_{12} normalized to remote uniaxial transverse stress are summarized in Figure 28. The trend of increasing local stresses concentration with the rise of peak misalignment angle is maintained. The induced normal longitudinal stresses (σ_{11}) however are significantly affected, which can be attributed to a rise in elastic modulus, since there is a ratio of $E_1/E_2 = 13,785$. This time, not only the shear stresses will be significant in terms of failure, but also the normal transverse stresses.

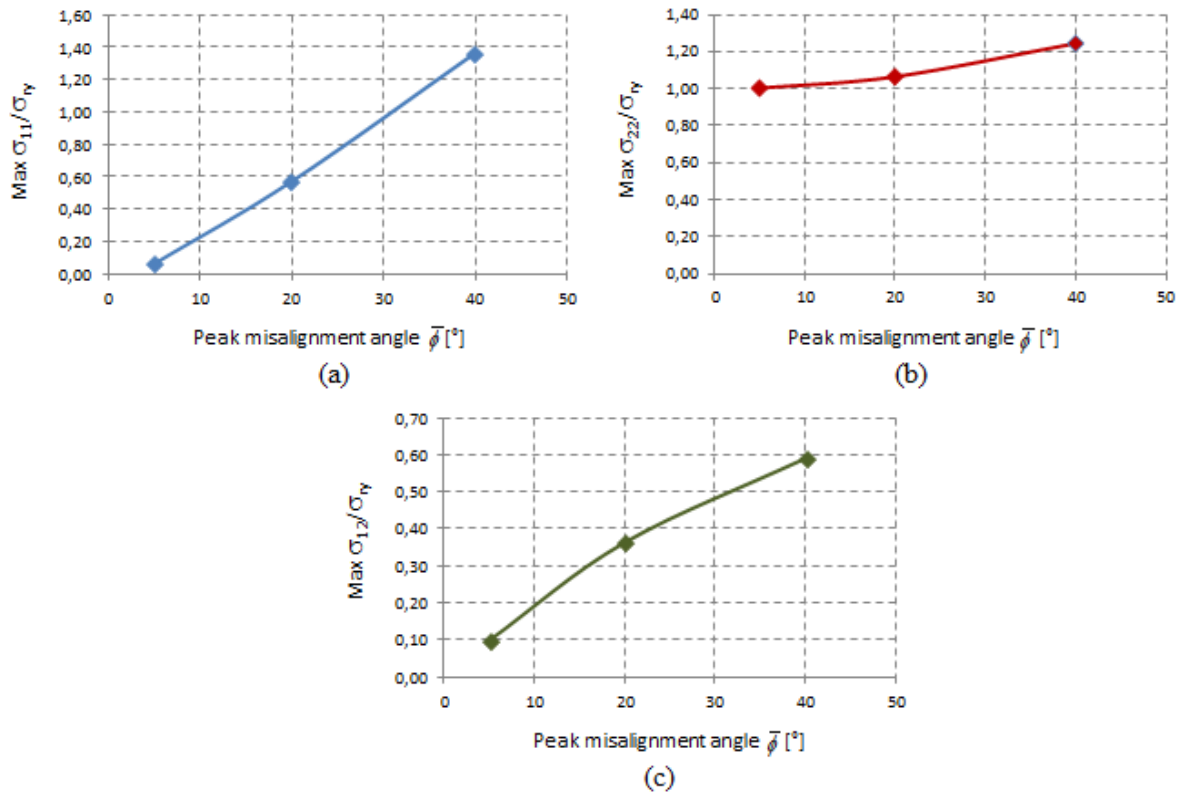


Figure 28 – Maximum normalized stresses for uniaxially transverse loaded laminae as a function of peak misalignment angle ($\bar{\phi}$).

HFC indices examination shows that failure will be initiated by matrix compression index for compressive loading, as presented in Figure 29, while for tensile loading matrix tension index will be the critical one. The nature of the stress that will govern failure as well as the localization of its initiation point depends on the loading sign. Tensile loaded laminae present failure dominated by transverse stress concentration, which is more significant in the region right above the peak of the central wave. Compressive loaded laminae have failure dominated by shear stresses which maximum values are once again localized in regions with maximum fiber inclination. Details are presented in “Appendix: Simulation detailed results – Critical HFC index examination”.

Figure 30 presents the initial failure strength reduction for the uniaxial normal transverse loaded laminae as a function of the peak misalignment angle. Once again the results are separated for tensile and compressive cases and shown as a percentage ratio of the strengths of the lamina with central waviness with respect to the lamina with perfectly straight and aligned fibers. The strength knock-down variation here observed proved to be less significant

than the ones obtained by longitudinal loaded laminae (Figure 26). Tensile cases were less affected by the waviness defect than compressive cases.

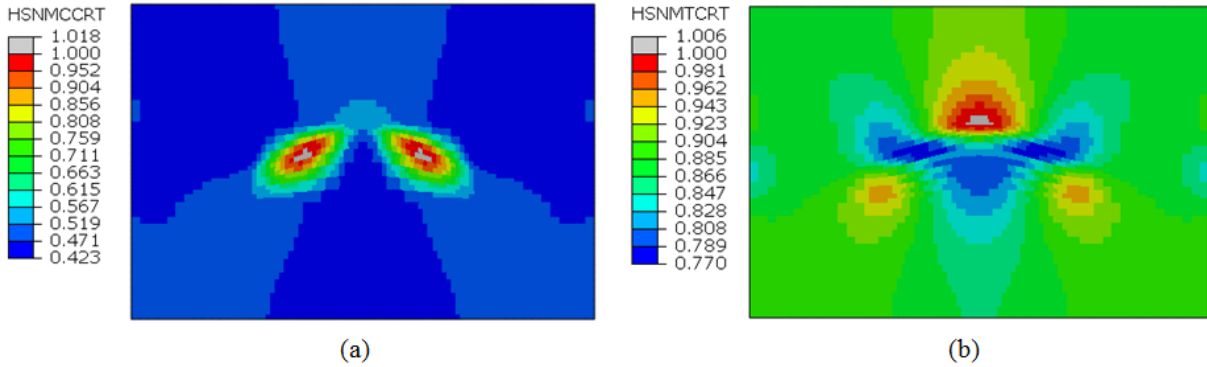


Figure 29 – Hashin critical failure indices for a lamina with $\bar{\phi} = 20^\circ$ in-plane central waviness at initial failure: (a) Matrix compression index for a lamina under transverse compression; (b) Matrix tension index for a lamina under transverse tension.

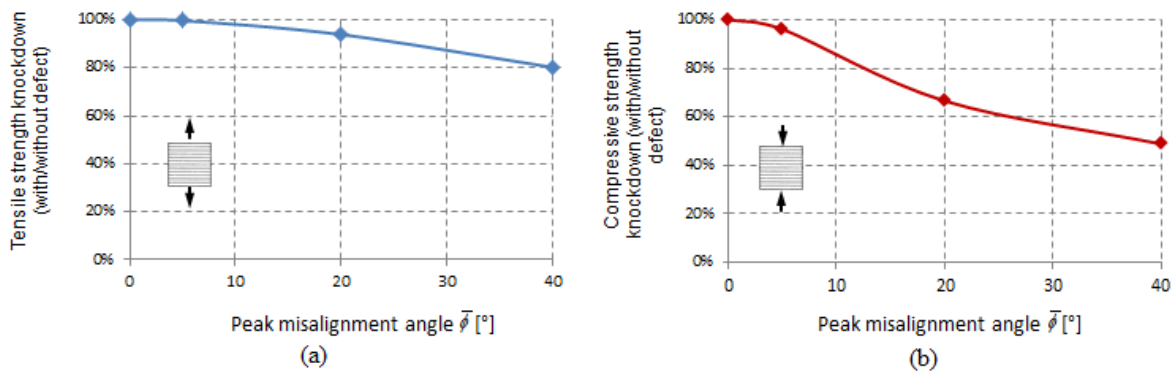


Figure 30 – (a) Transverse tensile and (b) transverse compressive initial failure strength ratio of the lamina with central waviness normalized with respect to the lamina with no defect.

4.3 Biaxial normal loaded laminae

Lamina local plane stresses of a lamina in the presence of central FW for both uniaxial and biaxial loading are presented in Figure 32-Figure 34, following the load identification scheme proposed on Figure 31. The resulting stress field for the biaxial loading cases proved to be a combination of the stress states generated by each individual uniaxial case (longitudinal and transverse), as expected for linear elastic analyses. It is very important to point that a resulting “marcelling pattern” for shear stress is also obtained for biaxial normal loads.

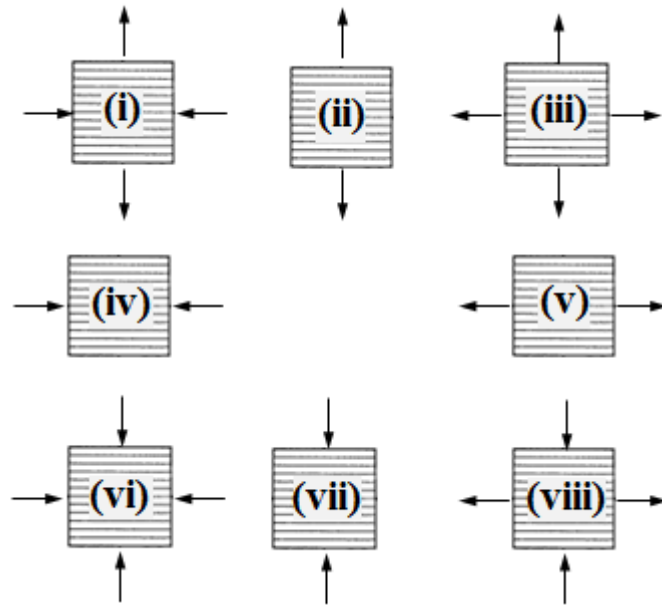


Figure 31 – Legend for load case identification of Figure 32Figure 37.

HFC analyses shows that failure will be governed by matrix indices associated with the acting transverse loading, according to Figure 35. This is once again explained by the fact that CFRP composites are quite sensitive to transverse and shear stresses because the associated strengths are typically an order of magnitude lower than longitudinal strength. That means that biaxial loading cases of longitudinal tension + transverse tension (load case (iii), according to the legend of Figure 31) and longitudinal compression + transverse tension (i) will fail by matrix tension index. Laminae under longitudinal tension + transverse compression (viii) and longitudinal compression + transverse compression (vi) will have failure defined by matrix compression index.

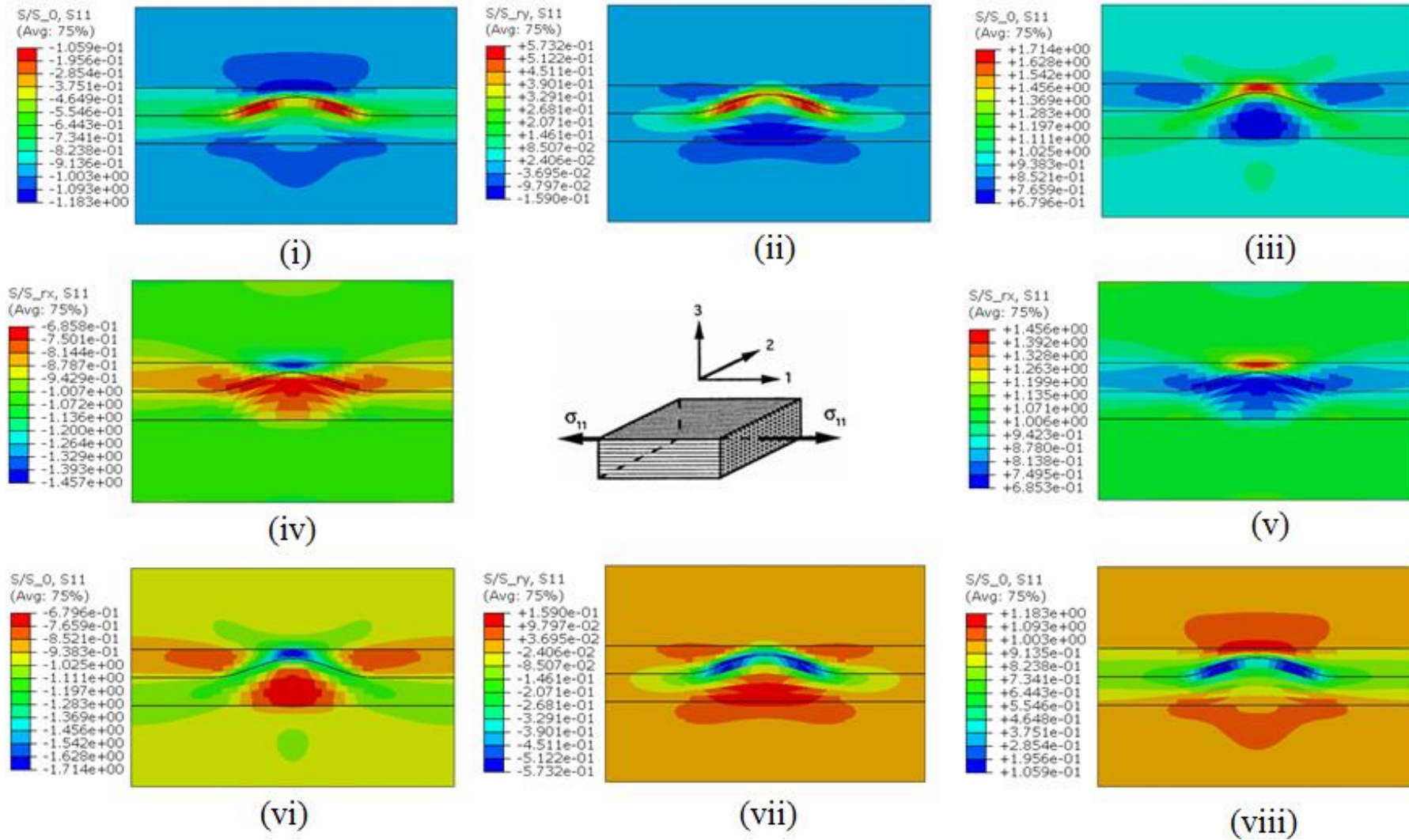


Figure 32 – Normal longitudinal stress in local 1-direction (σ_{11}) for a lamina with $\bar{\phi} = 20^\circ$ in-plane waviness, under uniaxial and biaxial responses.

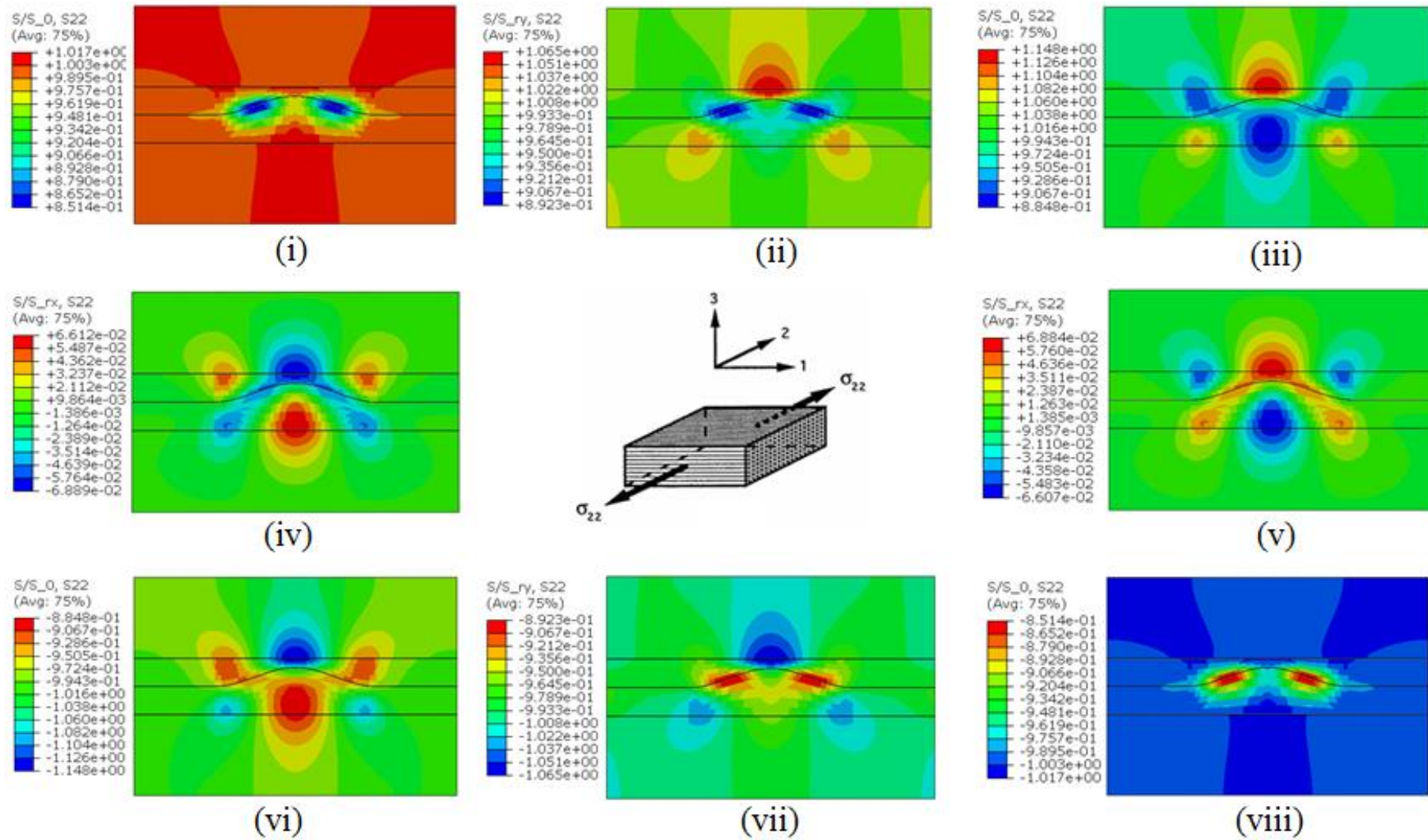


Figure 33 – Normal transverse stress in local 2-direction (σ_{22}) for a lamina with $\bar{\phi} = 20^\circ$ in-plane waviness, under uniaxial and biaxial responses.

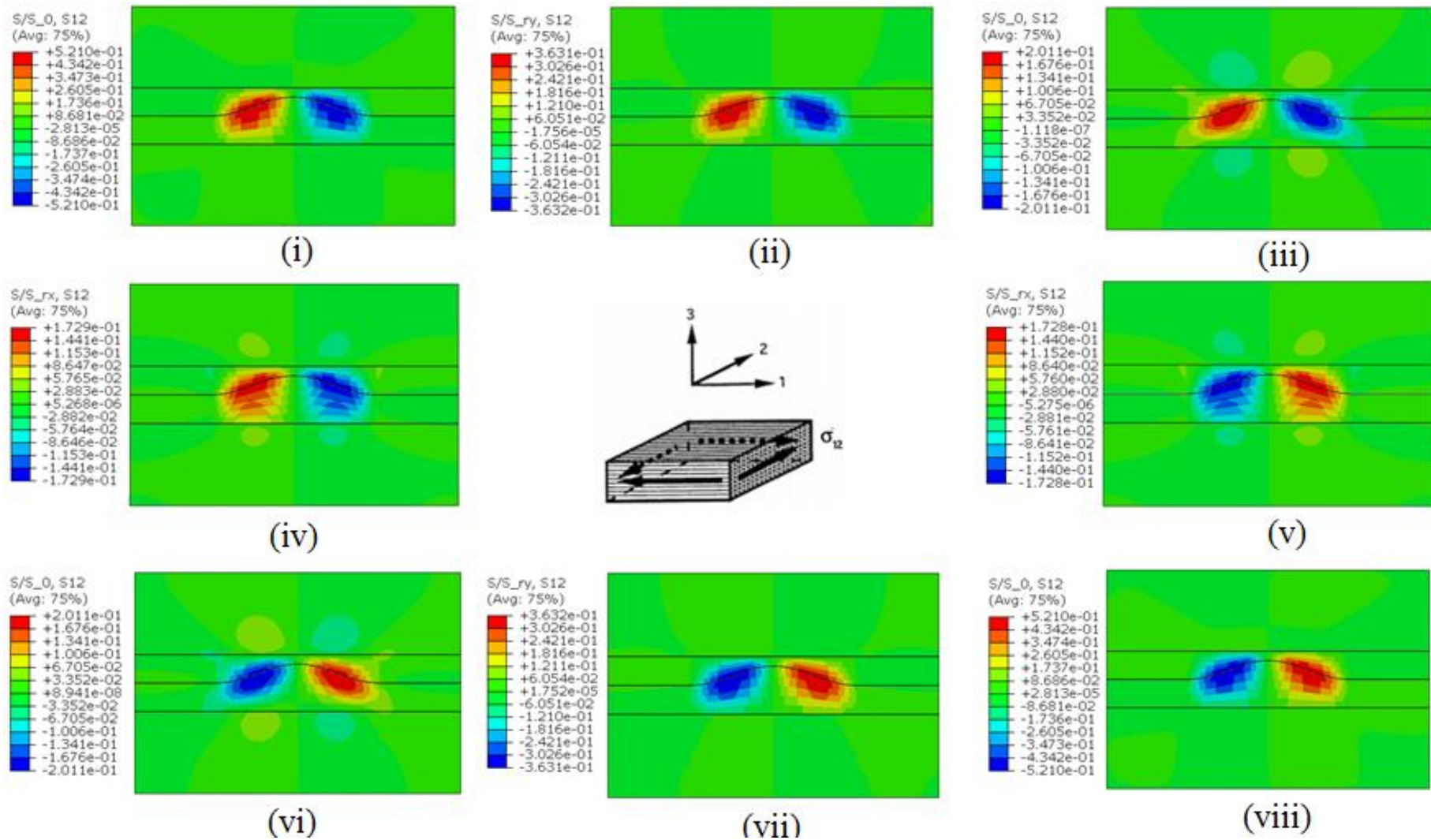


Figure 34 – In-plane shear stress in local 12-direction (σ_{12}) for a lamina with $\bar{\phi} = 20^\circ$ in-plane waviness, under uniaxial and biaxial responses.

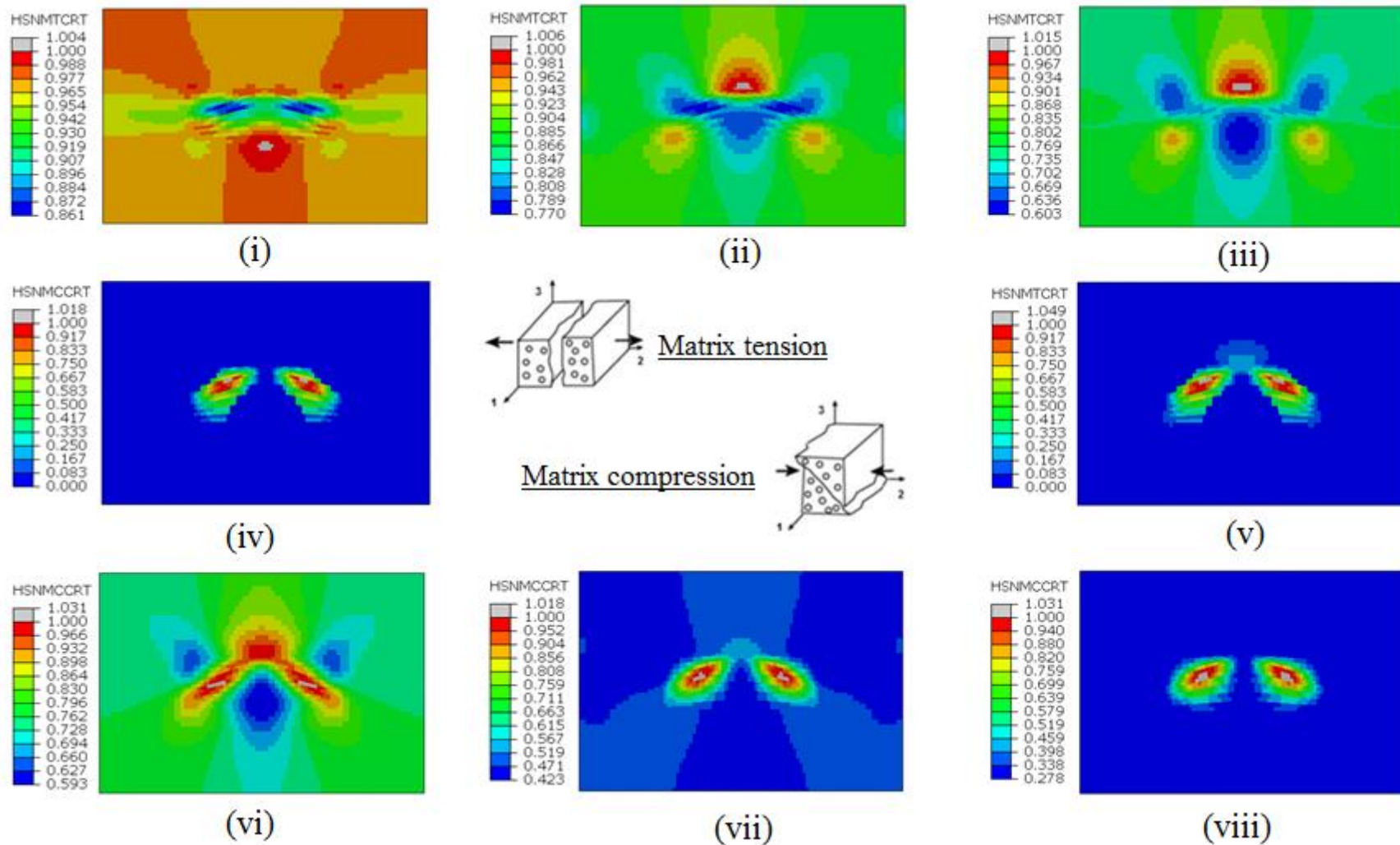


Figure 35 – Hashin critical failure indices for a lamina with $\bar{\phi} = 20^\circ$ in-plane waviness at initial failure, under uniaxial and biaxial responses. Matrix compression index for load cases (iv), (vi), (vii) and (viii); Matrix tension index for load cases (i), (ii), (iii) and (v).

Biaxial strength reduction for laminae with different peak misalignment angle values in comparison with laminae with perfectly straightly aligned fibers is presented in Figure 36. The biaxial load case of longitudinal tension + transverse compression was the most severely affected, as it presents a combination of higher allowable strength values in both longitudinal and transverse directions. Longitudinal compression + transverse tension case on the other hand was the least susceptible one, since it is associated with a pair of lower allowable strength).

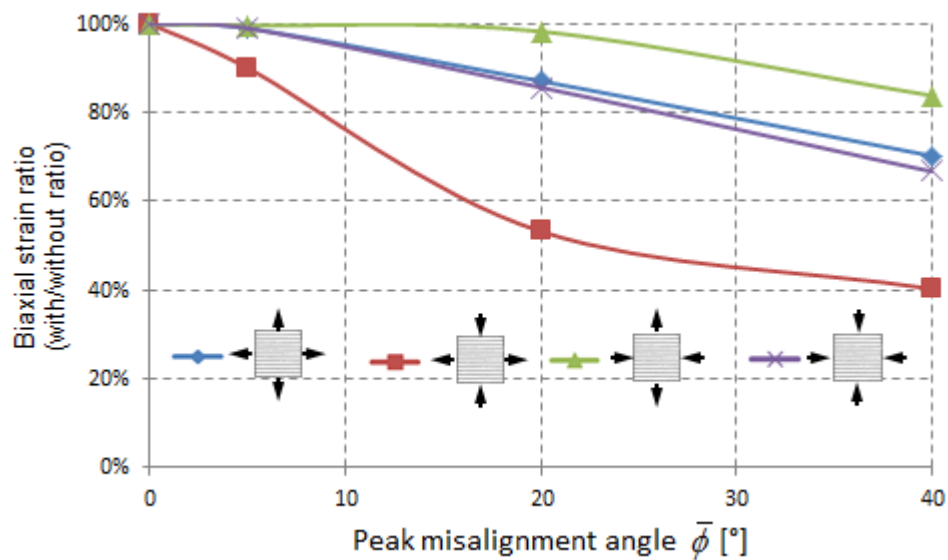


Figure 36 – Initial biaxial failure strain ratio of laminae with central waviness normalized with respect to laminae with no defect.

5

CONCLUSIONS AND RECOMMENDATIONS

5.1 Conclusions

Once that fiber waviness is a manufacturing defect that can not be entirely avoided, it is of vital importance to understand the mechanical behavior transformations experienced in the presence of these alterations.

Apparent longitudinal stiffness was little affected by in-plane waviness; the influence on apparent stiffness was negligible.

In-plane waviness proved to have an effect on local stiffness, affecting the stress field of the surrounding region. For uniaxial longitudinal loaded specimens, waviness causes the occurrence of normal transverse and in-plane shear stresses and a change in longitudinal stresses distribution. For uniaxial transverse loaded laminae, there is the emergence of normal longitudinal and also shear stresses, with a change in transverse stress distribution.

In terms of failure, the induced shear stresses favors a matrix dominated failure mode, as indicated by Hashin matrix indexes. This mode presents a much lower strength in comparison with straight fiber regions. The strength of a lamina in the presence of waviness is lower in comparison with a lamina with straightly aligned fibers (no defect). Longitudinal load cases present a higher strength knockdown than observed on transverse loading. This can be traced to a change in failure mode, that will be dominated by matrix strength.

The biaxial loading case of longitudinal tension + transverse compression was the most severely affected in terms of failure; biaxial loading with longitudinal compression + transverse tension was the least susceptible case.

As peak misalignment angle grows, the stronger these effects appear, leading to matrix cracking appearance. In general, reductions in stiffness were less significant than in strength.

This methodology provided a platform to study the behavior of wavy composites in a systematic manner. It can be extended to analyze several problems, including particular plane stress states of portions of larger structures.

5.2 Recommendations for future work

The author recommends that controlled experiments be conducted to verify this theory and its findings.

Manufacturing processes that may induce fiber waviness should be reexamined to select coupons.

Coupled in and out-of-plane waviness have been reported in literature. The three-dimensional stress state may reduce stiffness and strength of lamina and may also be investigated.

6

REFERENCES

ABOUDI, J.; ARNOLD, S.M.; BEDNARCYK, B.A. *Micromechanics of Composite Materials: A Generalized Multiscale Analysis Approach*. 1 ed. Oxford, UK: Elsevier Inc, 2012. 1006p. (ebook ISBN: [9780123977595](#)).

ALTMANN, A.; GESELL, P.; DRECHSLER, K. *Strength prediction of ply waviness in composite materials considering matrix dominated effects*. *Composite Structures* 127, pp. 51-59, 2015. (doi: [10.1016/j.compstruct.2015.02.024](#))

CAIAZZO, A.; ORLET, M.; McSHANE, H.; STRAIT, L.; RACHAU, C. *The effect of marcel defects on composite structural properties*. *Composite Structures: Theory and Practice*, ASTM STP 1383. West Conshohocken, PA. American Society for Testing and Materials. pp. 158-187, 2000.

CARLSSON, L.A.; ADAMS, D.F.; PIPES, R.B. *Basic experimental characterization of polymer matrix composite materials*. *Polymer Reviews*, Vol 53, 2013 – Issue 12. pp.277-302. 2013. (doi: [10.1080/15583724.2013.776588](#))

CHAKRAPANI, S.K.; BARNARD, D.; DAYAL, V. *Detection of in-plane fiber waviness in composite laminates using guided lamb modes*. 40th Annual Review of Progress in Quantitative Nondestructive Evaluation., pp. 1134-1140, 2014. (doi: [10.1063/1.4864948](#))

CIMINI JR, C.A.; TSAI, S.W. *Ply waviness on in-plane stiffness of composite laminates*. *Proceedings of the 12th International Conference on Composite Materials (ICCM-12)*, Paris, FR, 5-9 July, 1999. ICCM (International Council of Composite Materials), Paper 1346. pp.1-10, 1999. (<http://www.iccm-central.org/Proceedings/ICCM12proceedings/site/htmlpap/pap1346.htm>)

CIMINI JR, C.A. *Effect of Ply waviness on the in-plane stiffness of composite laminates*. 67p. Dissertation (Doctor of Philosophy in Aeronautics and Astronautics). Stanford University, Stanford, 1997.

DANIEL, I.M.; ISHAI, O. *Engineering Mechanics of Composite Materials*. 1 ed. New York. Oxford University Press, 1994. 395p. (ISBN: [0-19-507506-4](#))

ELHAJJAR, R.J.; SHAMS, S.S.; KEMENY, G.J.; STUESSY, G. *A Hybrid numerical and imaging approach for characterizing defects in composite structures*. Composites: part A 81. pp. 98-104, 2016. (doi: [10.1016/j.compositesa.2015.10.027](https://doi.org/10.1016/j.compositesa.2015.10.027))

EDGREN, F.; ASP, L.E. *Approximate analytical constitutive model for non-crimp fabric composites*. Composites: Part A 36. pp 173-181. 2005. (doi: [10.1016/j.compositesa.2004.06.007](https://doi.org/10.1016/j.compositesa.2004.06.007))

FARNAND, K.A. *Process-induced wrinkling and waviness in prepreg charge-forming*. 225p. Thesis. (Master of applied science in Materials Engineering). University of British Columbia (Vancouver), 2016.

GARNICH, M.R.; KARAMI, G. *Finite element micromechanics for stiffness and strength of wavy fiber composites*. Journal of Composite Materials, Vol 38, No 4. pp. 273-292, 2004. (doi: [10.1177/0021998304039270](https://doi.org/10.1177/0021998304039270))

HALLANDER, P.; AKERMO, M.; MATTEI, C.; PETERSSON, M.; NYMAN, T. *An experimental study of mechanisms behind wrinkle development during forming of composite laminates*. Composites: Part A 50. pp. 54-64, 2013. (doi: [10.1016/j.compositesa.2013.03.013](https://doi.org/10.1016/j.compositesa.2013.03.013))

HASHIN, Z.. *Failure criteria for unidirectional fiber composites*, Journal of Applied Mechanics, 47(2), 1980, pp. 329-334 (doi:[10.1115/1.3153664](https://doi.org/10.1115/1.3153664))

HSIAO, H.M.; DANIEL, I.M. *Effect of fiber waviness on stiffness and strength reduction of unidirectional composites under compressive loading*. Composites Science and Technology 56. pp. 581-593, 1996. (doi: [10.1016/0266-3538\(96\)00045-0](https://doi.org/10.1016/0266-3538(96)00045-0))

KARAMI, G.; GARNICH, M. *Effective moduli and failure considerations for composites with periodic fiber waviness*. Composite Structures 67. pp. 461-475, 2005. (doi:[10.1016/j.compstruct.2004.02.005](https://doi.org/10.1016/j.compstruct.2004.02.005))

KUGLER, D; MOON, T.J. *Identification of the most significant processing parameters on the development of fiber waviness in thin laminates*. Journal of Composite Materials 36 (12): pp. 1451-79, 2002. (doi: [10.1177/0021998302036012575](https://doi.org/10.1177/0021998302036012575))

LEMANSKI, S.L.; SUTCLIFFE, M.P.F. *Compressive failure of finite size unidirectional composite laminates with a region of fibre waviness*. Composites: Part A 43. pp. 435-444, 2012. (doi: [10.1016/j.compositesa.2011.11.007](https://doi.org/10.1016/j.compositesa.2011.11.007))

MALLICK, P.K. *Composites Engineering Handbook*. New York. Marcel Dekker Inc, 1997. 1249p. (ISBN: [0824793048](https://www.isbn-international.org/number/0824793048))

MANDELL. J.J.; SAMBORSKY, D.D.; WANG, L. *Effects of fiber waviness on composites for wind turbine blades*. International SAMPE (Society for the Advancement of Material and Processing Engineering) Symposium and Exhibition, Long Beach, USA, 12-16 May, 2003, pp. 2653-2666. (<http://www.montana.edu/composites/documents/SAMPE%202003%20paper.pdf>)

MIZUKAMI, K.; MIZUTANI, Y.; TODOROKI, A.; SUZUKI, Y. *Detection of in-plane and out-of-plane fiber waviness in unidirectional carbon fiber reinforced composites using eddy current testing*. pp.84-94. 2016. (doi: [10.1016/j.compositesb.2015.09.041](https://doi.org/10.1016/j.compositesb.2015.09.041))

PAIN, D.; DRINKWATER, B.W. *Detection of fibre waviness using ultrasonic array scattering data*. Journal of Nondestructive Evaluation; 32(3), pp. 215-227, 2013. (doi: [10.1007/s10921-013-0174-z](https://doi.org/10.1007/s10921-013-0174-z))

POTTER, K. *Understanding the origins of defects and variability in composites manufacture*. Proceedings of the 17th International Conference on Composite Materials (ICCM-17). Edinburg, UK. 27-31 July 2009. ICCM (International Council of Composite Materials), Plenary P1.5, pp.1-19, 2009. (<http://iccm-central.org/Proceedings/ICCM17proceedings/Themes/Plenaries/P1.5%20Potter.pdf>)

POTTER, K.; KHAN, B.; WISNOM, M.; BELL, T.; STEVENS, J. *Variability, fibre waviness and misalignment in the determination of the properties of composite materials and structures*. Composites: Part A 39. pp.1343-1354, 2008. (doi: [10.1016/j.compositesa.2008.04.016](https://doi.org/10.1016/j.compositesa.2008.04.016))

SALABERGER, D.; KANNAPPAN, J.A; KASTNER, J.; REUSSNER, J.; AUINGER, T. *Evaluation of computed tomography data from fibre reinforced polymers to determine fibre length distribution*. Int Polym Process 26. pp. 283-291. 2011. (doi: [10.3139/217.2441](https://doi.org/10.3139/217.2441))

SHAMS, S; ELHAJJAR, R.F. *Investigation into the effects of waviness in standard notched composite specimens*. CEAS Aeronaut J 6:541-555. 2015. (doi: [10.1007/s13272-015-0161-4](https://doi.org/10.1007/s13272-015-0161-4))

SJÖLANDER, J.; HALLANDER, P.; AKERMO, M. *Forming induced wrinkling of composite laminates: A numerical study on wrinkling mechanism*. Composites: Part A 81. pp. 41-51, 2016. (doi: [10.1016/j.compositesa.2015.10.012](https://doi.org/10.1016/j.compositesa.2015.10.012))

SUTCLIFFE, M.P.F; LEMANSKI, S.L; SCOTT, A.E. *Measurement of fibre waviness in industrial composite components*. Composites Science and Technology 72. pp. 2016-2023. 2012. (doi: [10.106/j.compscitech.2012.09.001](https://doi.org/10.106/j.compscitech.2012.09.001))

YURGATIS, S.W. *Measurement of small angle misalignments in continuous fibre composites*. Composites Science and Technology 30, pp. 279-293. 1987. (doi: [10.1016/0266-3538\(87\)90016-9](https://doi.org/10.1016/0266-3538(87)90016-9))

Appendices

SIMULATION DETAILED RESULTS – STRESS DISTRIBUTION

Uniaxial normal longitudinal loaded laminae

According to chapter 4.1, simulations of laminae under uniaxial normal longitudinal load were performed for the moderate ($\bar{\phi} = 5^\circ$), severe ($\bar{\phi} = 20^\circ$) and very severe ($\bar{\phi} = 40^\circ$) defects. Detailed results for moderate and very severe defects (not shown in chapter 4.1) are described below.

Very severe defects ($\bar{\phi} = 40^\circ$)

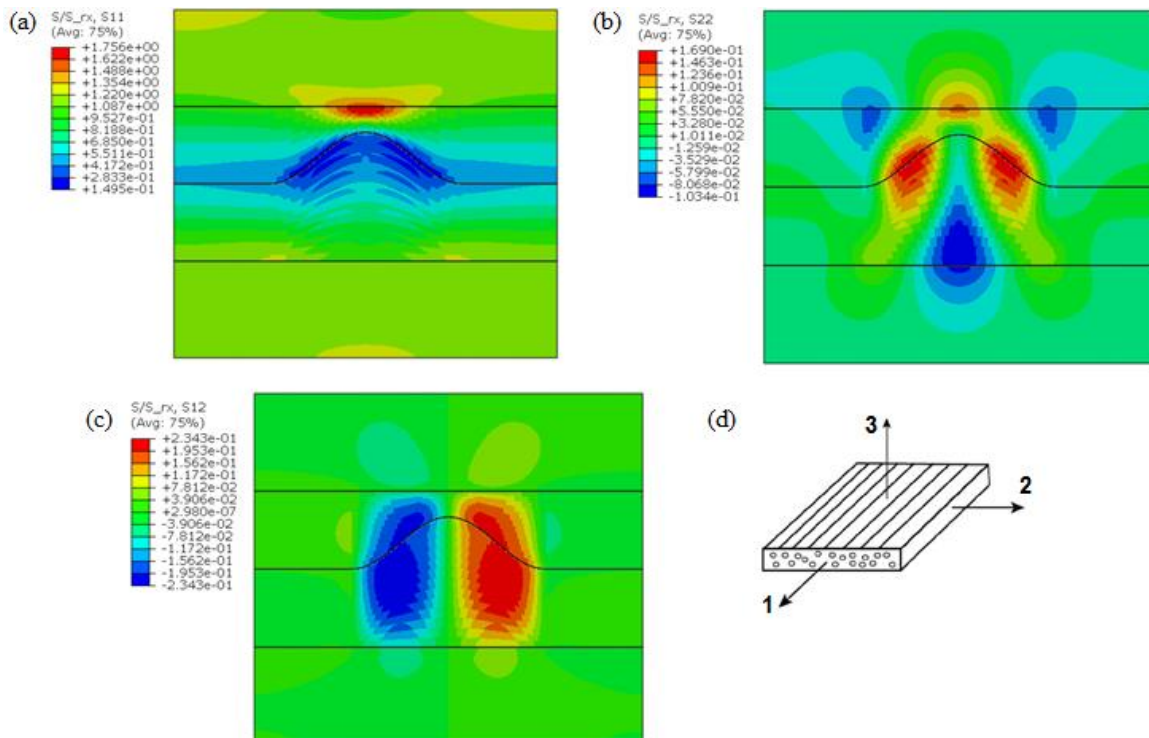


Figure 37 – Linear elastic stress fields normalized to remote stress σ_{rx} for lamina with $\bar{\phi} = 40^\circ$ in-plane waviness under uniaxial normal longitudinal loading: (a) normal longitudinal stress in local 1-direction σ_{11} , (b) normal transverse stress in local 2-direction σ_{22} , (c) local in-plane shear stress in 12-direction σ_{12} , and (d) local coordinate axes.

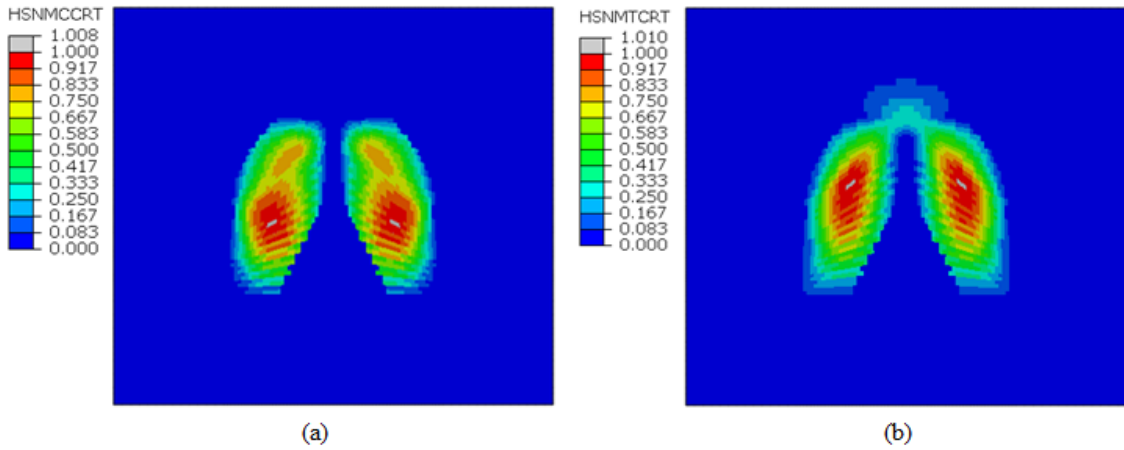


Figure 38 – Hashin critical failure indices for a lamina with $\bar{\phi} = 40^\circ$ in-plane central waviness at initial failure: (a) Matrix compression index for a lamina under longitudinal compression; (b) Matrix tension index for a lamina under longitudinal tension.

Moderate defects ($\bar{\phi} = 5^\circ$)

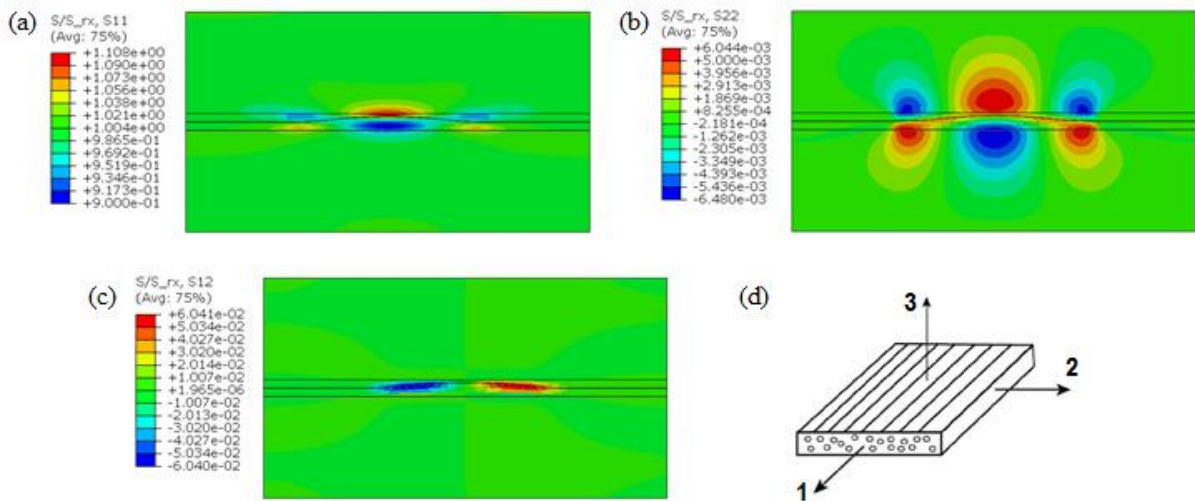


Figure 39 – Linear elastic stress fields normalized to remote stress σ_{rx} for lamina with $\bar{\phi} = 5^\circ$ in-plane waviness under uniaxial normal longitudinal loading: (a) normal longitudinal stress in local 1-direction σ_{11} , (b) normal transverse stress in local 2-direction σ_{22} , (c) local in-plane shear stress in 12-direction σ_{12} , and (d) local coordinate axes.

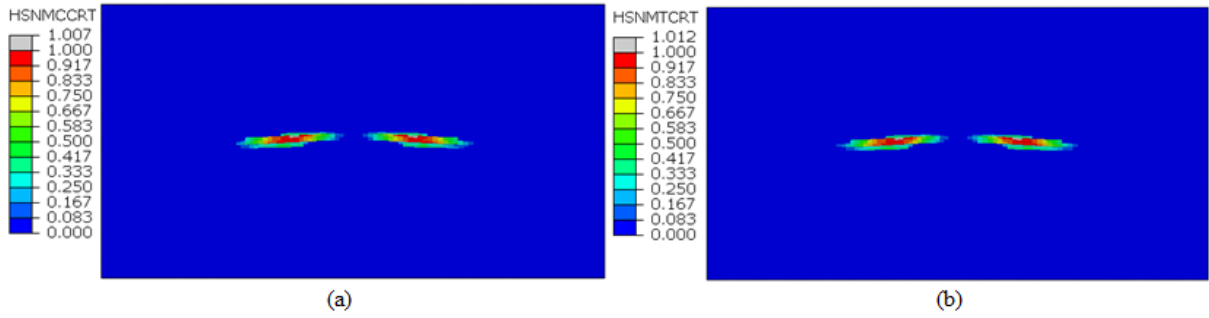


Figure 40 – Hashin critical failure indices for a lamina with $\bar{\phi} = 5^\circ$ in-plane central waviness at initial failure:
 (a) Matrix compression index for a lamina under longitudinal compression; (b) Matrix tension index for a lamina under longitudinal tension.

Uniaxial normal transverse loaded laminae

According to chapter 4.2, simulations of laminae under uniaxial normal transverse load were once again performed for the moderate ($\bar{\phi} = 5^\circ$), severe ($\bar{\phi} = 20^\circ$) and very severe ($\bar{\phi} = 40^\circ$) defects. Detailed results for moderate and very severe defects are described below.

Very severe defects ($\bar{\phi} = 40^\circ$)

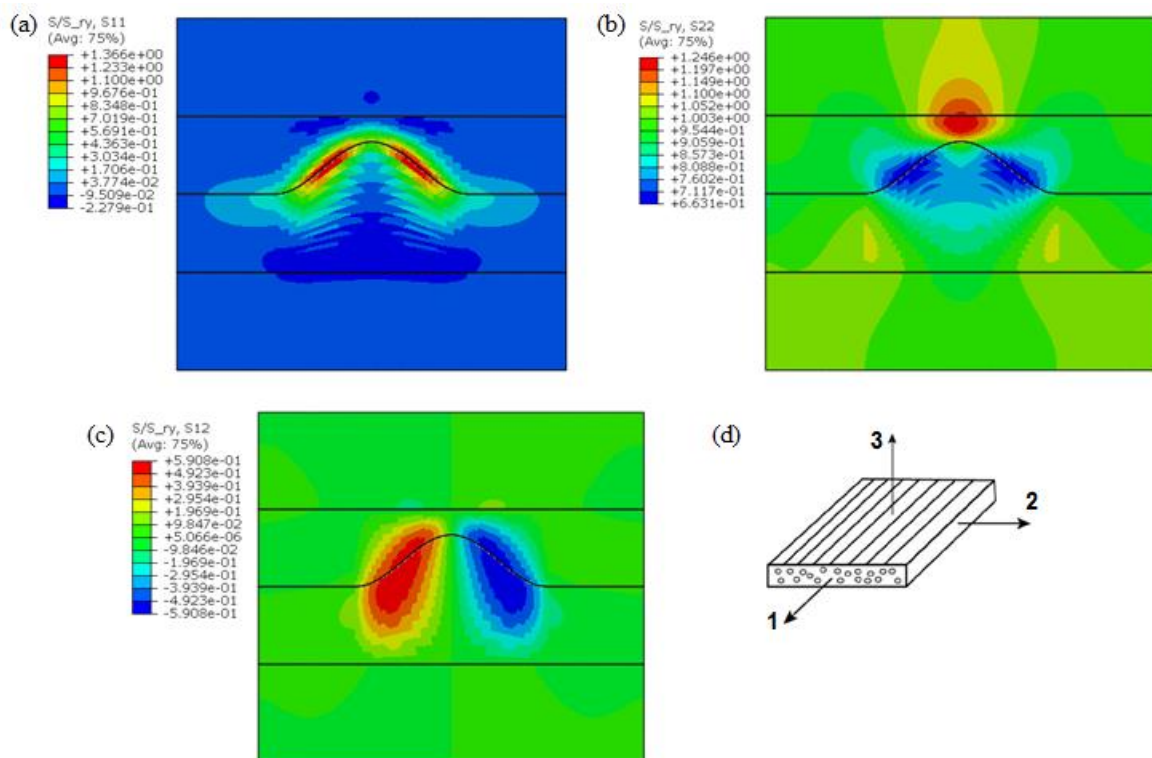


Figure 41 – Linear elastic stress fields normalized to remote stress σ_{ry} for lamina with $\bar{\phi} = 40^\circ$ in-plane waviness under uniaxial normal transverse loading: (a) normal longitudinal stress in local 1-direction σ_{11} , (b) normal transverse stress in local 2-direction σ_{22} , (c) local in-plane shear stress in 12-direction σ_{12} , and (d) local coordinate axes.

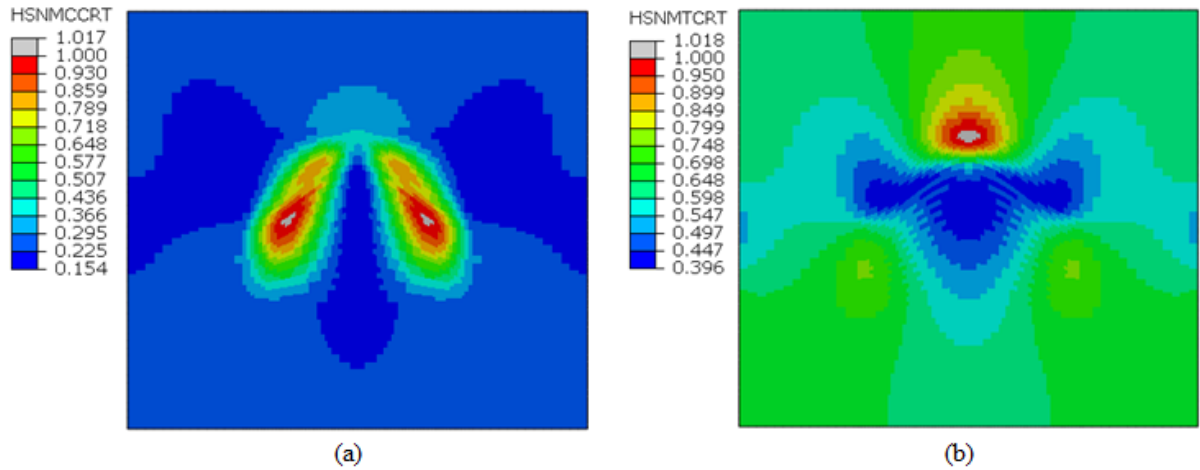


Figure 42 – Hashin critical failure indices for a lamina with $\bar{\phi} = 40^\circ$ in-plane central waviness at initial failure: (a) Matrix compression index for a lamina under transverse compression; (b) Matrix tension index for a lamina under transverse tension.

Moderate defects ($\bar{\phi} = 5^\circ$)

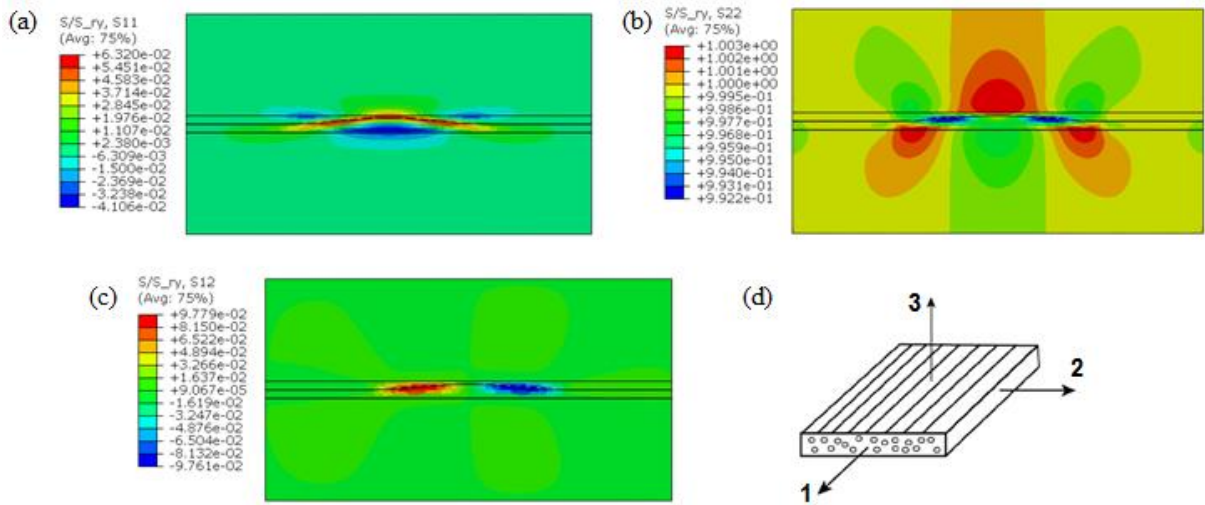


Figure 43 – Linear elastic stress fields normalized to remote stress σ_{ry} for lamina with $\bar{\phi} = 5^\circ$ in-plane waviness under uniaxial normal transverse loading: (a) normal longitudinal stress in local 1-direction σ_{11} , (b) normal transverse stress in local 2-direction σ_{22} , (c) local in-plane shear stress in 12-direction σ_{12} , and (d) local coordinate axes.

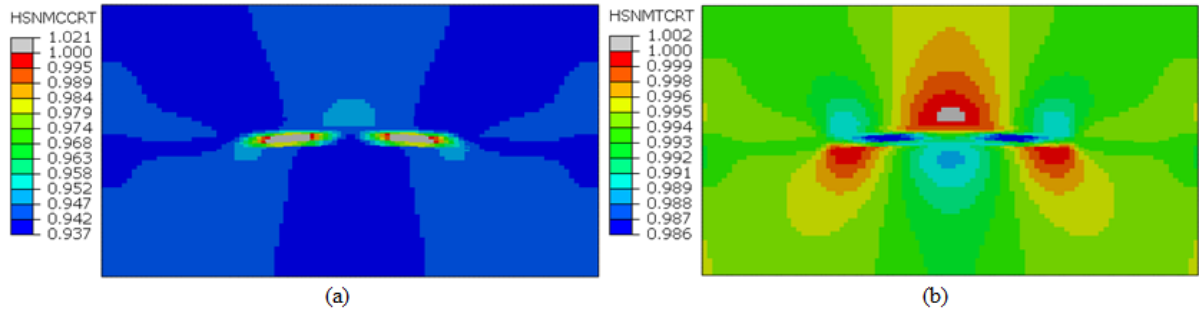


Figure 44 – Hashin critical failure indices for a lamina with $\bar{\phi} = 5^\circ$ in-plane central waviness at initial failure:
 (a) Matrix compression index for a lamina under transverse compression; (b) Matrix tension index for a lamina under transverse tension.

SIMULATION DETAILED RESULTS – CRITICAL HFC INDEX EXAMINATION

The following tables present how the critical HFC index for each individual simulation is composed of, in terms of normal (compression or tension) and shear stresses. The results are separated in moderate ($\bar{\phi} = 5^\circ$), severe ($\bar{\phi} = 20^\circ$) and very severe defects ($\bar{\phi} = 40^\circ$), under uniaxial and biaxial loading. Once again, the load identification scheme proposed on Figure 31 (chapter 4.3) was used.

Very severe defects ($\bar{\phi} = 40^\circ$)

Table 5 – Critical Hashin failure criterion index composition for a lamina with $\bar{\phi} = 40^\circ$ in-plane central waviness, under uniaxial and biaxial responses.

Load ID	Critical Failure Index	Critical index fraction due to normal stresses [%]	Critical index fraction due to in plane shear stresses [%]
(i)	Matrix Tension	99,915	0,085
(ii)	Matrix Tension	99,984	0,016
(iii)	Matrix Tension	100,000	<0,001
(iv)	Matrix Compression	2,428	97,572
(v)	Matrix Tension	51,674	48,326
(vi)	Matrix Compression	34,262	65,738
(vii)	Matrix Compression	14,110	85,890
(viii)	Matrix Compression	7,762	92,238

Severe defects ($\bar{\phi} = 20^\circ$)

Table 6 – Critical Hashin failure criterion index composition for a lamina with $\bar{\phi} = 20^\circ$ in-plane central waviness, under uniaxial and biaxial responses.

Load ID	Critical Failure Index	Critical index fraction due to normal stresses [%]	Critical Index fraction due to in plane shear stresses [%]
(i)	Matrix Tension	100,000	<0,001
(ii)	Matrix Tension	99,998	0,002
(iii)	Matrix Tension	100,000	<0,001
(iv)	Matrix Compression	0,685	99,315
(v)	Matrix Tension	9,937	90,063
(vi)	Matrix Compression	70,117	29,883
(vii)	Matrix Compression	37,218	62,782

(viii)	Matrix Compression	20,788	79,212
--------	--------------------	--------	--------

Moderate defects ($\bar{\phi} = 5^\circ$)

Table 7 – Critical Hashin failure criterion index composition for a lamina with $\bar{\phi} = 5^\circ$ in-plane central waviness, under uniaxial and biaxial responses.

Load ID	Critical Failure Index	Critical index fraction due to normal stresses [%]	Critical index fraction due to in plane shear stresses [%]
(i)	Matrix Tension	100,000	<0,001
(ii)	Matrix Tension	99,999	0,001
(iii)	Matrix Tension	100,000	<0,001
(iv)	Matrix Compression	0,034	99,966
(v)	Matrix Tension	0,538	99,462
(vi)	Matrix Compression	100,000	<0,001
(vii)	Matrix Compression	90,870	9,130
(viii)	Matrix Compression	79,115	20,885